Electronic Thesis and Dissertation Repository

11-30-2021 2:30 PM

Modeling Fetal Brain Development: A semi-automated platform for localization, reconstruction, and segmentation of the fetal brain on MRI

Jianan Wang, *The University of Western Ontario*

Supervisor: Duerden, Emma G., *The University of Western Ontario*
A thesis submitted in partial fulfillment of the requirements for the Master of Engineering
Science degree in Biomedical Engineering
© Jianan Wang 2021

Follow this and additional works at: https://ir.lib.uwo.ca/etd

Part of the Developmental Neuroscience Commons

Abstract

With advances in fetal magnetic resonance imaging (MRI), research in neonatal neuroscience has shifted to identify *in utero* brain-based biomarkers for outcome prediction in high-risk fetuses, particularly those impacted by growth restriction. Volumetric segmentation of the fetal brain can provide better understanding of the trajectories of brain development and may aid in predicting functional outcomes. The current thesis aimed to develop semi-automatic methods to target deep brain structures in the fetal brain identified on MR images in fetuses with and without growth restriction. In this study, pregnant women (35-39 weeks gestational age [n=9]) with growth appropriate (n=8) and growth restricted fetuses (n=1) were recruited. Fetal MRI was performed on 1.5 Tesla (T) and 3T MRI scanners and 2D stacks of T2-weighted images were acquired. A novel fetal whole brain segmentation algorithm developed for second trimester fetuses was applied to the T2-weighted MR images to reconstruct 2D volumes into 3D images. To segment deep brain structures, an atlas of cortical and subcortical structures was registered to the 3D reconstructed images. Linear and nonlinear registration algorithms, with two types of similarity metrics (mutual information [MI], cross-correlation [CC]), were compared to determine the optimal strategy of segmenting subcortical structures. Dice similarity coefficients were calculated to validate the reliability of automatic methods and to compare the performance between the registration algorithms compared to manual segmentations. Comparing atlas-generated masks against manually segmented masks of the same brain structures, the median Dice similarity coefficients for linear registration using CC performed optimally. However, post hoc analyses indicated that linear MI and CC performed comparably. Overall, this semi-automatic subcortical segmentation method for third-trimester fetal brain images provides reliable performance. This segmentation pipeline can aid in identifying early predictors of brain dysmaturation to support clinical decision making for antenatal treatment strategies and promote optimal neurodevelopment in fetuses.

Keywords

Fetal neurodevelopment, Neurodevelopmental disorder, Fetal MRI, Fetal growth restriction, Fetal brain segmentation, Subcortical segmentation, Nonlinear registration, Linear registration.

Summary for a Lay Audience

Each year, over 30 million pregnancies are impacted by growth restriction, which is associated with delayed brain development, and may place newborns at risk for the later development of childhood psychiatric disorders as well as movement disabilities. Brain growth is a key marker for growth restriction as well as other disorders that can influence brain development. Better tools are needed to measure the growth of the fetal brain to aid in diagnosing and predicting developmental outcomes. Magnetic resonance (MR) imaging is an emerging tool to study the developing brain *in utero*. Presently manual labeling of brain regions in MR images is time consuming and costly, and automated methods are needed to rapidly target brain regions for brain growth study.

This thesis aimed to develop methods to facilitate the targeting of deep brain structures in the fetal brain identified on MR images in fetuses with and without growth restriction. To achieve this aim, a platform of novel algorithms that was designed to rebuild brain images corrupted by fetal motion, was evaluated. To study the brain growth, an atlas that labeled the brain regions was applied to the fetal images using an automated algorithm. To validate the atlas, two brain regions were manually outlined on the images. We compared the manually defined regions with five methods of automated segmentation. The different methods of automated segmentation varied in terms of the methods used to identify and align the features in the atlas with fetal images as well as their computing time. An automated method that uses a dense deformable image registration, where the goal is to identify corresponding areas between the atlas and fetal images, was as appropriate as a more computationally intensive method.

This semi-automated platform can be applied to identify fetuses with delayed brain growth as well as track growth over time during the third trimester to provide an image-based marker of brain health. This method can be further validated in larger samples in fetuses impacted by growth restriction. Studying brain growth in the fetus may aid in informing medical decision making for clinicians as well as improve counseling for families.

Acknowledgements

Table of Contents

List of Tables

List of Figures

List of Appendices

Acronyms

2D: Two-dimensional

3D: Three-dimensional

ANTs: Advanced Normalization Tools

ANTs Lin MI: ANTs linear registration with mutual information similarity metric

ANTs Lin CC: ANTs linear registration with cross correlation similarity metric

ANTs NL MI: ANTs nonlinear registration with mutual information similarity metric

ANTs NL CC: ANTs nonlinear registration with cross correlation similarity metric

CSF: Cerebro-spinal Fluid

CNN: convolutional neural network

FGR: fetal growth restriction

FLIRT: FMRIB's Linear Image Registration Tool

FSE: fast spin echo

IUGR: Intrauterine Growth Restriction

HASTE: HAlf fourier Single-shot Turbo spin-Echo

MRI: Magnetic Resonance Imaging

TR: repetition time

TE: echo time

SyN: Symmetric Image Normalization

1   Chapter One

1.1   Introduction

Magnetic resonance imaging (MRI) of the fetal brain for clinical purposes has advanced

considerably in recent years due to its application in assessing atypical brain development,

brain injury and potential utility to predict functional outcomes in high-risk fetuses.

Additionally, research-based MRI studies of typical fetal brain development have provided

important normative data for subsequent comparison with clinical populations. MRI methods

for the characterization of fetal brain abnormalities are of key clinical relevance due to the

high incidence of central nervous system malformations (i.e., anencephaly, ventriculomegaly,

schizencephaly, callosal agenesis) in as many as 1/1000 fetuses (Werner et al., 2018). In

particular, detection of delayed brain growth associated with fetal conditions such as

intrauterine growth restriction (IUGR) or preterm birth offers new opportunities to identify

objective biomarkers that can facilitate better understanding of fetal brain development as

well as improved management of high-risk pregnancies (Rutherford et al., 2008; Wu et al.,

2020), and potentially early detection of neurodevelopmental disorders (Banović et al., 2014;

Bonnet-Brilhault et al., 2018). Additionally longitudinal studies point to fetal brain

abnormalities as an important contributor to later life neurodevelopmental and psychiatric

disorders (Thomason, 2020). Delayed neonatal brain development is associated with

neurodevelopmental disorders, such as autism spectrum disorder (Makropoulos et al., 2018).

Better understanding of the trajectories of fetal brain development may aid in predicting fetal

functional outcomes and later learning difficulties and neurodevelopmental disorders.

Research in neonatal development has shifted to an earlier window of maturation, the

fetal period, to identify *in utero* brain-based biomarkers. With advances in fetal MRI,

quantitative neuroimaging has been increasingly applied to study fetal brain growth and neurodevelopment. Segmentation of the fetal brain into its grey and white matter subcomponents can provide insight into fetal brain dysmaturation, attributed to maternal placental insufficiency and subsequent fetal growth restriction. Quantitative measurements of fetal brain and subcortical volumes can support characterizing normal brain development and identifying early predictors of brain dysmaturity, which is critical for developing antenatal treatment strategies to better support fetal neurodevelopment and neonatal outcomes (Rathbone et al., 2011;Boardman et al., 2010). However, the traditional manual segmentation of MR images is time consuming and requires high level expertise, thus it is impractical to implement these methods to large datasets. Therefore, reliable automatic segmentation methods for fetal MR images are needed in order to study typical and atypical fetal brain development.

Automatic segmentation pipelines and routines developed for neonatal and child imaging protocols are not appropriate for the study of fetal brain tissue. Namely, the acquisition of fetal MR images is dependent upon rapid acquisition of high in-plane resolution images and must undergo reconstruction to develop a three-dimensional (3D) MR image. The 3D image can subsequently be segmented into its grey and white matter constituents parts using an age-appropriate atlas (Gholipour et al., 2017).

To segment the fetal brain, the newly published NiftyMIC automatic brain segmentation algorithm (Ebner et al., 2020), developed using second trimester MRI scans, will be applied to T2-weighted MR images acquired during the third trimester. The NiftyMIC algorithm relies on 'stacks' of 2D images acquired in the three image planes (i.e., axial, coronal, sagittal). The three sets of images can be acquired rapidly (Kuklisova-Murgasova et al., 2012).

To perform the regional segmentation of the cortex and subcortical areas in the fetal brain after the whole brain segmentation, we applied two atlas-based segmentation techniques, a linear and a nonlinear atlas registration algorithm. Atlas-based segmentation methods have been used to target deep brain structures in fetal MR images. Landmark-based rigid image transformation has been applied to fetal MR images to obtain volumetric and cortical measures with acceptable performance (Wu et al., 2020). However nonlinear registrations are more robust and may be able to more accurately segment subcortical structures in fetal MR images compared to linear registration. We examined whether more computationally intensive nonlinear image registration is needed for adequate subcortical segmentation performance compared to linear image registration. The goal of this research was to develop and implement a semi-automatic pipeline combining automatic fetal brain segmentation, volumetric reconstruction, and atlas registration algorithms for subcortical segmentation in fetal brains to extract and analyze subcortical volumes.

1.2   Background

1.2.1   Fetal brain development

The development of the human brain begins in the embryonic stage, in the third week of gestation with the formation of the neural tube. Once the neural tube closes the embryo further develops the central nervous system by extensive progenitor cell proliferation, cellular migration, and expansion to form the cortical layers in a genetically predetermined pattern. During the first trimester of embryonic and fetal development, the cells which line the neural tube, the neuroepithelial cells, undergo symmetric division to further populate the pool of cells to form the developing nervous system (Figure 1-1). The neural epithelial cells extend and transform into radial glial cells. The radial glial cells are essential for cortical layering. These specialized cells form the scaffolding for the cortical layers. By the end of

the first trimester, the radial glial cells generate neuroblasts, which are precursor cells that can become neurons and glial cells. The neurons form the cortical and subcortical grey matter, and the glial cells support the neurons and form the white matter of the brain. The cortical and subcortical grey matter is formed by progenitor cells in the neural tube. The progenitor cells later become the neurons and glia that form the foundation of central nervous system. The glial cells permit the developing neurons to migrate to genetically determined locations to form the cortical layers (Moffat et al., 2015). Neural and glial cells in the linings of the vesicles begin to organize and form the layers of the cortex. These vesicles that later form the telencephalon, begin to develop in the 5th week of gestation. This stage is referred to as the 5th vesicle stage. The five vesicles include the lateral ventricles, the third ventricle and the fourth ventricle. In this stage, the early beginnings of the telencephalon and diencephalon (cortex, white matter, basal ganglia and thalamus, hypothalamus), the mesencephalon (midbrain), the rhombencephalon (pons, cerebellum) begin to form. The telencephalon will later develop into the cerebral cortex while the rhombencephalon will later develop into the brainstem and cerebellum.
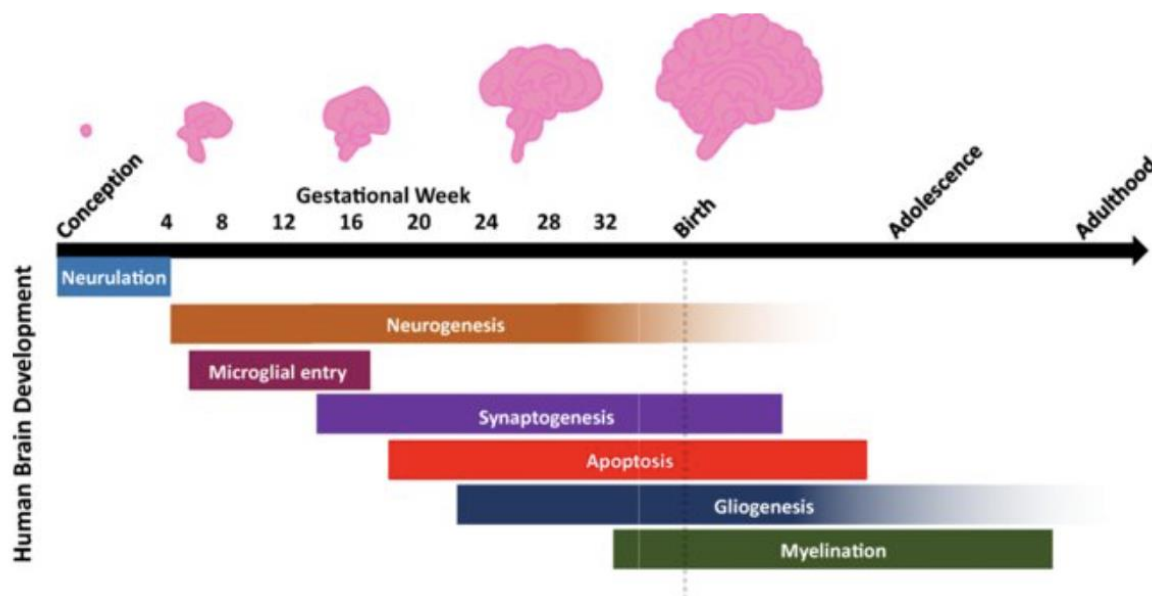
Figure 1-1: Timeline of early brain development. Brain development in the begins during embryogenesis at two to three weeks with the formation of the neural tube (neurulation). Following neurulation is the development of new neurons (neurogenesis). New neurons are produced till just after birth. The formation of connections or synapses amongst neurons (synaptogenesis) occurs at 12 weeks. At 18 gestational weeks, programmed cell death (apoptosis) removes extra synapses and cells. This is to ensure proper development and synaptic connectivity in the developing brain. At 22 gestational weeks, specialized cells (glial cells) needed for neuronal migration to develop the cortex (gliogenesis). At 32 weeks, the glial cells also promote the formation of myelination of the neurons, which allows for efficient communication among neurons. This process of myelination to enhance brain connectivity continues well after the newborn period into the third decade of life. Adapted from Schnoll et al. 2021 (Open Access).

1.2.2   Placental insufficiency and fetal growth restriction (FGR)

Recent studies suggest that neurodevelopmental disorders, such as autism spectrum disorder (ASD), attention deficit hyperactive disorder (ADHD), and obsessive-compulsive disorder (OCD) have their origins *in utero* (Straughen et al., 2017). As such, there is a growing interest in exploring the role of the placenta and cerebral oxygen delivery from the mother to the fetus in the etiology of neurodevelopmental disorders.

The placenta is located at the interface of the mother and fetus (Chen et al., 2020). During pregnancy, the placenta is an important source of nutrients, hormones, and

inflammatory factories in fetal circulations. Medical disorders of pregnancy can impact placental function and fetal outcomes. Impaired uteroplacental function, such as inadequate blood flow to the placenta causing the fetus to receive inadequate amount of nutrients and oxygen will result in slowing or even cessation of fetal growth, which is termed as placental insufficiency (Browne et al., 2015; Cetin & Antonazzo, 2009).

Placental insufficient is a direct cause of fetal growth restriction (FGR). It contributes to up to 40% of FGR cases (Cetin & Antonazzo, 2009). FGR is a serious pregnancy complication affecting about 8% of pregnancies in the US (Damhuis et al., 2021). This number is even bigger in developing countries, such as Sub-Saharan Africa and Southeast Asia due to the unsustainable resource of nutrients during pregnancy (Black et al., 2017). For fetuses who have restricted growth, they can have abnormally small dimensions of their bodies and lower birth weights compared to growth-appropriate fetuses. The current Canadian clinical determination of FGR is an estimated fetal weight in the 10th percentile or lower (Sharma et al., 2016). Some placental disorders that lead to restricted nutrient delivery are maternal obesity, pregestational diabetes, maternal depression, and maternal infection during pregnancy (Fleiss et al., 2019).

1.2.3   FGR and placental function and neurodevelopmental disorders
Evidence suggests that neurodevelopmental disorders are associated with medical disorders of pregnancy. Previous studies reported that preterm birth, FGR, and low birth weight are associated with varied structural and functional brain maturation, cognitive and behavioral deficits, and neurodevelopmental impairments (Nosarti et al., 2012; Sacchi et al., 2020). Specifically, for low-birthweight infants, they have a four-fold higher risk of perinatal death

and worse neurodevelopmental outcomes including alterations in brain volume (Miller et al., 2016).

Czarzasta and colleagues (Czarzasta et al., 2019; Czarzasta et al., 2020) reported in preclinical rodent models, that maternal depression, which is often comorbid with cardiovascular disease, can cause also growth, neurodevelopmental and behavioral delays in offspring. There is an increased risk of neurodevelopmental disorders among growth restricted fetuses whose mothers have placental diseases. In a meta-analysis (Zauche et al. 2017) it was demonstrated that advanced parental age at birth, bleeding during pregnancy, gestational diabetes, and prematurity were associated with an to an increase risk of later developing ASD. Also, maternal obesity, gestational diabetes, preeclampsia, placental insufficiency, low maternal education, young maternal age, and prematurity are associated with a higher risk of language and cognitive delays as well as ADHD. However, few studies were exploring whether there is significant brain injury or delayed brain development of fetuses during pregnancy. There also lacks quantitative analysis and methods of brain volumetric differences between fetuses with and without FGR.

1.2.4   *MRI of the fetal brain*

Fetal ultrasonography has been a primary tool for the clinical diagnosis of fetal brain abnormalities. Over the last two decades, significant headway has been made in fetal Magnetic Resonance Imaging (MRI) protocols that have enabled rapid advances in the characterization of typical and atypical brain development *in utero*. Over the last 2 decades research in fetal MRI protocols has increasingly been used to non-invasively study the functional, metabolic and structural origins of the fetal brain in vivo (Thomason et al., 2015;

Thomason et al., 2018; Wheelock et al., 2019; Pradhan et al., 2020; Turk et al., 2019);

however, uncertainty remains about the extent of diagnostic and clinical impact of fetal MRI.

Advances in structural MRI protocols to study grey and white matter development,

and toolboxes have been developed for processing and analyzing volumetric data. These

protocols and toolboxes have the potential to rapidly advance MRI as an adjunct clinical tool

to improve diagnostic accuracy and to provide adequate counseling and prognostication.

Furthermore, fetal MRI studies offer a unique window into second and third trimester brain

development, which can be used as reference values for neonatal brain maturation in the case

of preterm birth. Fetal brain imaging methodology is quickly advancing in terms of ultrafast

imaging, motion-insensitive sequences and preprocessing tools to manage motion corrupted

images. Technological advances in fetal MRI methods have the potential to identify image-

based biomarkers within this important developmental window, and in conjunction with

other diagnostic imaging tools, fetal MRI holds the potential for precision health in the fetus.

Numerous issues in fetal MRI set it apart from imaging studies with children or

adults. The first MRI study of the fetus was reported in the early 1980s (Smith et al., 1983).

Subsequent early MRI examinations focused on fetal and placenta structure and function in

clinical settings. The increase in fetal MRI in recent years has shown that it is an important

method in early identification, intervention, and treatment of developmental disorders and

disease. For example, phase-contrast and T2-weighted MRI has demonstrated that fetal brain

volume is significantly smaller in fetuses with congenital heart disease due to reduced

cerebral oxygenation (Sun et al., 2015), which may underlie delayed brain maturation and the

increased incidence of brain injury seen in this population (Barkhuizen et al., 2021).

Motion is an issue in child and adult neuroimaging; however, child and adult head

motions can be minimized through foam padding around the head and neck during MRI

scanning. The fetus depending on their gestational age and weight, can move significantly during the course of a single MRI acquisition for a number of reasons, including fetal head and limb movement as well maternal breathing and heart rate (Malamateniou., 2013). Motion during fetal MRI acquisition produces large artifacts in the data, impacting the ability to determine the differences in the grey and white matter tissue or even rendering the MRI data unusable (Ferrazzi et al., 2014).

Methods and techniques have been developed in order to prevent, minimize, and correct fetal motion (Robinson & Ederies, 2018). A good method employed by several groups to reduce fetal motion is to aim to scan the fetus at a predicted time they will be asleep (Malamateniou et al., 2013; Robinson & Ederies, 2018). However, research is also equivocal on whether fetuses move less in the morning compared to the afternoon (Avitan et al., 2018; Patrick et al., 1978).

Ensuring that the mother is comfortable in the scanner, as well as minimizing stress or feelings of claustrophobia in the mother can reduce fetal motion. Coaching the mothers in advance on the necessity of staying still during the scan and practicing breath-holding methods are demonstrated techniques to minimize maternal and subsequent fetal movement, which can aid in reducing motion artifacts in the data. Maternal short-term fasting as well as minimizing caffeine intake prior to the scan can minimize fetal movement (Devoe et al., 1986, 1993; Mirghani et al., 2003).

Scanning at later gestational ages can also aid with minimizing fetal motion as the more weight the fetus puts on and turns head down in preparation for birth, the less likely the fetus will have space in the uterus to move (Koshida et al., 2019; Lockwood Estrin et al., 2012; Pearson & Weaver, 1977; Sadovsky & Yaffe, 1973). However, some studies have

reported that third trimester fetuses move comparably to second trimester fetuses (Connors et al., 1988; Valentin & Marŝál, 1986).

While there are few methods to prevent fetal motion that create distortions in the MR images, specific imaging protocols can be used to minimize the effect of motion on MR image quality. These protocols focus on reducing the time it takes to acquire an anatomical scan, as faster acquisitions provide less time for fetal motion to occur.

The imaging protocol most commonly used in fetal MRI is fast spin echo (FSE). In a typical spin echo sequence, one echo is measured per repetition time (TR). In FSE, multiple echoes are measured per TR, reducing the number of TRs, and therefore the length of the scan, to collect a full volume that covers the fetus. In the case of fetal imaging, a full volume can be acquired in a single TR, in a sequence called HASTE (HAlf fourier Single-shot Turbo spin-Echo) or single-shot FSE (Prayer et al., 2004; Robinson & Ederies, 2018).

Fetal white matter is developing exponentially in the third trimester. In turn, the axons in the fetal brain are thinly myelinated and the white matter contains significantly more water than adult brains. Having a long echo time (TE) in T2-weighted sequences can best capture this contrast between the white and grey matter. Despite requiring a longer TE than T1-weighted sequences, they are still shorter than traditional 3D volumes acquired in children and adults, minimizing the time to complete a scan and therefore the possibility of motion corruption. One caveat however is that these images are captured in high resolution only in a single plane, with two low-resolution out-of-plane images. While the in-plane images are generally robust against motion corruption, the two out-of-plane images are particularly susceptible (Malamateniou et al., 2013). Once the MRI images have been collected, significant motion correction during the processing stages is often required.

1.2.5 Fetal brain segmentation and volumetric reconstruction algorithms

Deep learning techniques has shown preferable performance in the field of image segmentation. The convolutional neural network (CNN) is one of the most implemented techniques among various deep learning algorithms. CNN has been applied for volumetric segmentation of many different medical images, such as 3D (three-dimensional) infant brain MR image segmentation (Zhang et al., 2015), skull stripping of 3D MR images among adult population (Carré et al., 2020; Kleesiek et al., 2016), blood vessel segmentation in retinal images, skin cancer segmentation, and lung lesion segmentation (Alom et al., 2019). However, the fetal MR image segmentation is considerably more challenging than image segmentation among more mature populations in terms of MR image acquisitions and morphological processing mainly because of inevitable fetal motion and possible maternal motion. The ideal imaging sequence for scanning fetuses is different, and the acquired fetal MR images were in the form of stacks of two-dimensional (2D) low resolution images. It is challenging to apply typical 3D CNN techniques for adult MR brain images on prenatal MR images for high fidelity fetal brain segmentation. Therefore, our dataset required a segmentation algorithm for 2D (in axial, sagittal, and coronal planes) images and volumetric reconstruction from 2D planes into 3D radiological anatomical planes, which is important for visualizing the white and grey matter for neuroradiological evaluation, and is critical for longitudinal comparison between typically-developing and growth restricted fetuses.

Slice-to-volume reconstruction (SVR; Rousseau et al., 2006) is one technique in which multiple high-resolution 2D steady state FSE images are combined to form a single, high resolution 3D image, which can subsequently be registered with an age-appropriate atlas for volumetric segmentation. SVR is based on the assumption that all images are centered over a single organ (e.g., the brain), and that the three orthogonal directions (i.e., axial,

sagittal, and coronal) are covered. One low resolution image is used as a reference, and the remaining low-resolution images are aligned to form a single high-resolution 3D volume. Next, each slice is re-aligned to the high-resolution volume, forming a motion-corrected 3D volume.

A newer technique that builds on SVR is Patch-to-Volume Reconstruction (PVR). While SVR is able to correct for rigid-body motion such as rotation and translation, PVR treats the data as having rigid patches, allowing for the correction of non-rigid tissue motion (Alansary et al., 2017). Freely-available automated toolboxes for each technique have been made available by several groups, including PVR (Alansary et al., 2017), SVR (Kuklisova-Murgasova et al., 2012) and NiftyMIC (https://github.com/gift-surg/NiftyMIC; Ebner et al., 2020).

The newly developed novel fetal brain segmentation algorithm, NiftyMIC (Ebner et al., 2020) delivers a localization algorithm to target a box containing the fetal brain in the MR image in addition to the fetal brain segmentation and 3D volumetric reconstruction algorithms. This is important as the position and orientation of the fetus may vary among participants. Targeting a broad location in the fetal MR image aids in robustness for more challenging segmentation routines (Ebner et al., 2020) compared to segmentation methods without a fetal brain localization step (Rajchl et al., 2016; Salehi et al., 2018). This localization step uses a 2D CNN (P-Net by Want, 2018) to get an initial coarse fetal brain segmentation after down-sampling the input 2D slices to size of 96 by 96 pixels (Ebner et al., 2020). The morphological closing and opening operations are applied. This is done to reduce the number of small blank pixels in the territory of the fetal brain. The final 3D bounding box is obtained from the processed coarse segmentation and upscaled into the original space (Ebner et al., 2020).

For the final fetal brain segmentation step, the same 2D CNN (P-Net) is trained with a multi-scale loss function that calculates the similarity between the prediction and the "ground truth". The average similarity among a defined number of scales of the prediction against the group truth. The different scales for CNN layers are constructed by average pooling. The multi-scale loss function was developed by Ebner et al. (2020), which compared Dice loss and logistic loss functions, the relationship between adjacent pixels is additionally considered to increase the similarity across scales. The segmented stacks of 2D slices are then bias corrected. One of the low-resolution segmented stacks of 2D slices is randomly selected as the target stack. The remaining 2D stacks are intensity corrected according to and rigidly registered to the selected stack. The slices are applied with nearest neighbor sampling and Gaussian blurring operation for an initial reconstructed high-resolution 3D volume and mask. Then the volume and mask are updated by iteratively applying rigid registration to the stacks to align with the previously established high-resolution volume for motion correction. Lastly the reconstructed 3D volume is rigidly registered into the standard anatomical space of a spatiotemporal atlas of healthy brains.

1.2.6   Registration-based subcortical segmentation

In this work, we focused on exploring antenatal subcortical growth of deep brain structures including the cerebellum and thalamus. The cerebellum and thalamus are key deep brain structures related to alterations in neuro-cognition and motor behaviors that are typically seen in infants impacted by FGF as well as preterm birth. Early growth impairments or alterations in the trajectory of growth in the cerebellum have been found to be associated with an increased risk of autism (Beversdorf et al., 2005; Limperopoulos et al., 2007). Further, cerebellar lesions in adulthood can impair decision-making, working memory, and planning

(Clausi et al., 2015; Koziol et al., 2014). Deficits in linguistic abilities, anxiety, and impaired social behavior have also been associated with cerebellar lesions (Ramphal et al., 2021; Schmahmann, 2004). Early cerebellar lesions at the vermis area can produce impaired eye gaze, anxiety, and lack of mental flexibility such as stereotyped behaviour (Clausi et al., 2015; Wells et al., 2008). The thalamus, is the primary relay station to the cortex and plays an important role in motor and cognitive functions (Dehghani & Wimmer, 2019). Atypical development of the thalamus is associated with impaired emotional processing, language, and social cognition in children and adult populations with neurodevelopmental disorders (Hardan et al., 2006). Volumetric segmentations of the cerebellum and thalamus can aid in morphological analysis of the growth of the two brain structures, which is beneficial to exploring the *in utero* origins of neurodevelopment disorders.

To segment the subcortical structures, we used image normalization techniques to linearly and nonlinearly register an age-appropriate fetal atlas into native space to determine an optimal strategy to segment subcortical structures. The segmented labels for brain tissue and structure including subcortical gray matter were rotated, moved, sheared, and scaled towards the subject image by rigid and affine registrations. Since the fetal brain grows rapidly during the third trimester of pregnancy and inter-slice fetal motions can lead to drastic inter-subject shape and volumetric differences, the template labels were further aligned with the subject brain using nonlinear registration. The packaged image normalization tools we used were compared with the well-known FSL (the FMRIB Software Library) library of tools, a platform-independent software package (Jenkinson et al., 2012) and the more computational expensive ANTs (Advanced Normalization Tools) suite of image registration tools. The linear image registration algorithms used were FLIRT (FMRIB's Linear Image Registration Tool) from the FSL platform and ANTs' rigid and

affine transformations. The nonlinear image registration algorithm used was SyN (Symmetric

Image Normalization) (Avants et al., 2008) from the ANTs platform. ANTs offers one of the

top-ranked performing nonlinear image registration algorithms (Klein et al., 2009). Different

similarity metrics, available within the ANTs suite of tools, affect the performance for inter-

or intra-modality image registrations. The fetal brain template and the subject scans were

both T2-weighted, however, the intensity signals of the subject images and the template

differed considerably. Therefore, testing and comparing image registration using different

similarity metrics, such as cross-correlation optimal for intra-modality registration and

mutual information optimal for both intra- and inter-modality registration were performed to

determine the optimal registration-based segmentation for our dataset.

1.3   Rationale

Few studies have assessed fetal brain development by analyzing the fetal brain volume

during the third trimester of pregnancy, despite its clinical relevance. Fetal motion is a

considerable issue when acquiring third trimester images. To mitigate motion artifacts, two

dimensional (2D) images are acquired in rapid succession in the 3 planes (coronal, sagittal,

axial). The NiftyMIC fetal brain reconstruction and segmentation algorithm that we

employed in this study was originally trained and tested on 2D second trimester fetal MR

images. Therefore, whether this deep-learning platform (NiftyMIC) can reliably segment

more mature and complex fetal brain tissue seen in the third trimester needs to be evaluated.

To examine regional subcortical organization of the fetal brain, MR images can be

registered into standardized space and previously published fetal brain atlases can be applied

to segment grey matter structures such as the thalamus and cerebellum. Atlas-based

segmentation techniques have been used for targeting deep brain structures in fetal MR

images; however, manual or rigid based segmentation methods are often employed, which are impractical to analyze large datasets and may provide inaccurate results due to improper characterization of the fetal brain anatomy. In this study, affine and nonlinear registration algorithms were compared to determine the optimal strategy of segmenting subcortical structures in T2-weighted images acquired during the third trimester of pregnancy. The affine algorithms included FLIRT (FMRIB's Linear Image Registration Tool) and the linear version of Automatic Normalization Tools (ANTs). The nonlinear registration methods included ANTs that employed different similarity metrics. FLIRT is a multi-start, multiresolution method that employs global optimization in order to determine an optimal affine transformation to minimize the differences between the atlas image and the fetal images. ANTs is a dense deformable image registration method that aligns images on a voxel-by-voxel basis. In general, dense deformable image registration is more computationally intensive. The decision to implement different methods (i.e., affine vs. nonlinear) for registration usually involves a trade-off between image registration quality and computation time. We therefore compared these different registration methods to determine the optimal registration strategy to apply a previously published fetal brain atlas to the individual fetal MRI scans in order to examine macrostructural development of subcortical structures.

1.4   Objectives and hypothesis

Following the workflow of the proposed automatic fetal subcortical segmentation, this study was separated into two aims. The first aim was to determine whether a deep-learning platform developed to reconstruct and segment the whole fetal brain in second-trimester fetal MR images can reliably segment images acquired in pregnant women during the third trimester. It was hypothesized that the deep-learning platform would reliably segment brain tissues in third-trimester MR images. The second aim was to determine whether an affine or

nonlinear registration produces optimal fetal subcortical segmentation. It was hypothesized that nonlinear registration of age-appropriate atlases of the fetal brain would result in more accurate segmentation of subcortical brain regions compared to linear registration methods.

2 Chapter Two

2.1 Methods

2.1.1 Participants

A total of nine pregnant adult women participated in the MRI study. All participants were in

the third trimester of ranging from 35 to 39 weeks of gestational age (GA). The average GA

was 36.6 weeks with standard deviation of 1.2 weeks (Table 2-1). Mothers pregnant with

singleton growth-appropriate or growth-restricted fetuses were recruited to the study. All

participants self-identified as native English speakers and reported no history of psychiatric

illness, neurological disorder, or hearing impairment. The study was approved by the Health

Sciences Research Ethics Board (REB# 109515) from Western University. The letter of

information was sent to participants in advance of the study and a member of the research

team reviewed the protocol. All participants provided informed consent.

Table 2-1: Median Maternal ages and fetal gestational ages

Characteristic	Total (n=9)
Maternal Age, Median years (IQR)	37.95 (34.30-41.2)
Fetal gestational age, Median weeks (IQR)	36.60 (36.10-37.30)

Ages of the mothers (years) and fetuses (weeks' gestation), IQR, interquartile range (25%ile-75%ile)

2.1.2 Procedure

All participants were invited to attend the MRI suite 15-20 minutes in advance of the scan

time in order to complete the screening form with the technologist, review all the safety

procedures and were provided with surgical scrubs to wear during the scan. Participants were

shown the MRI and the size of the scanning bore before entering the scanner. Participants

were informed about remaining still through the course of the experiment. Once participants

were familiarized with all procedures, they were then given information about the length of

the scanning protocol and the sounds they would be hearing. The MRI technologist and a

member of the research team informed the participants that they could signal that the scan be

stopped at any time by squeezing the alarm bell attached to the scanner bed. After all study

procedures and the protocol was reviewed with the participants, they were instructed to lay

on their left side on the scanner bed to minimize constriction of major arteries. All

participants were scanned while lying on their left side with their feet inside the scanning

bore. A body coil was placed over the participants before they were moved inside the scanner

bore.

2.1.3   MRI protocol

Participants were scanned at two sites different sites and the study procedures were

maintained at both scanning suites. Four participants were scanned on a 3T (General Electric

[GE], Milwaukee, WI; MR7500) MRI with a 32-channel GE torso coil and a 60 cm bore at

the Translational Imaging Research Facility at the Robarts Research Institute. The other five

participants were scanned on a 1.5 T (GE, MR450w) MRI with a GEM posterior and anterior

array coil with a 70 cm bore at London Health Research Science Center (LHSC-Victoria

Hospital). To shorten the MR image acquisition time considering mitigating motion artifacts

from fetal movements, the T2-weighted MR images were acquired using the single shot fast

spin echo (SSFSE) sequence (repetition time [TR] > 1200 msec, echo time [TE]: 81.36-93.60

msec, voxel size: $0.98*1.96*8$ mm^3 and $0.125*0.17*9$ mm^3). The fetal participants'

information including GA, volumes of subcortical regions of interest, and whole brain

volumes is presented in Table 2-1.

2.1.4 Study workflow
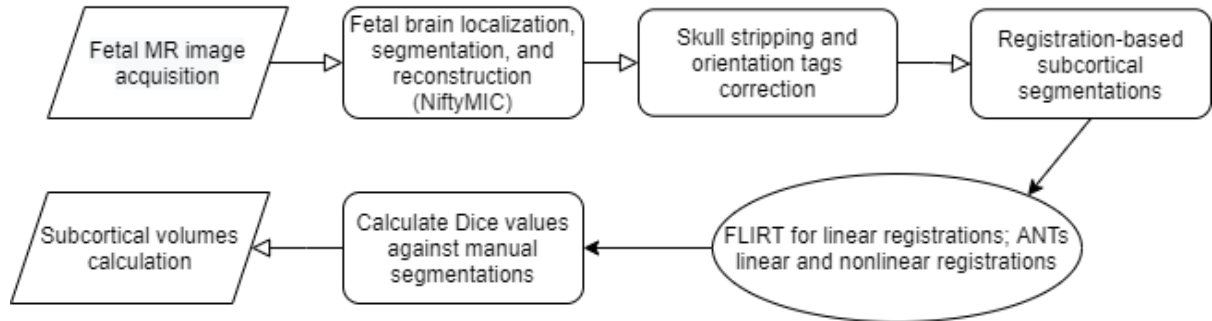
Figure 2-1: Study design flowchart. The study workflow included MR image acquisition, MR image preprocessing (registration, fetal deep brain structure segmentation) reliability testing and statistical analysis.

The study workflow (Figure 2-1) consisted of MR image acquisition, fetal MR image preprocessing including registration and fetal deep brain structure segmentation, reliability testing, and statistical analysis. The fetal MR images were first processed using NiftyMIC for fetal brain location detection, fetal brain segmentation, and volumetric reconstruction. The segmented brain masks underwent skull-stripping using the 3dcalc command line tool from AFNI toolkit (RW, 1996; RW et al., 1997). The skull-stripped brain volumes were manually corrected for orientation tags using ITK-SNAP. Both linear and nonlinear image registration algorithms were applied to an age-appropriate atlas (Gholipour et al. 2017). The resulting transformation matrices produced by the linear and nonlinear image registration algorithms from the different toolkits (FLIRT and ANTs) to register the atlas to the fetal T2 weighted images, were also used to register the manually segmented masks to the fetal images. The aligned subcortical labels were than compared with the manually segmented subcortical masks by calculating Dice Similarity coefficients using the convert3d command line tool from ITK-SNAP toolkit (Paul et al., 2006). The registered and segmented brain structures'

volumes were calculated and extracted using the fslstats command line tool from FSL

platform. Each step will be described in detail in the next subsections.

2.1.5   Fetal brain segmentation and volumetric reconstruction on MR images

In this step, NiftyMIC was used for broad fetal brain localization, precise fetal brain

segmentation, manual performance check and manually adjustment, manual orientation fix,

and auto skull stripping. The location of the fetal brain varied significantly across

participants, and the fetal brain represented only a small subsection of the 2D MR images,

the placenta and umbilical cord surrounding the fetal brain created a large source of non-

interested contents (Figure 2-2). In turn, large unrelated contents in the images could have

affected the robustness of the algorithm to differentiate the fetal brain from the rest of the

organs in the MR image and reconstruct the 2D input slices into 3D brain volumes.

Therefore, it was essential to first estimate the fetal brain location in the MR image such that

a bounding box (Figure 2-3) was created to reduce both unrelated contents and image space,

as well as the algorithm processing time for the later more precise fetal brain segmentation

algorithm using 2D P-Net CNN (Yamashita et al., 2018). After the broad fetal brain

localization, the input 2D MR images were segmented in three dimensions, the axial,

coronal, and sagittal planes; however, the surrounding maternal grey and white tissue was

still evident in the slices. The binary fetal brain masks (Figure 2-4), which served as input

binary masks for the later volumetric reconstruction algorithm to build 3D fetal brain masks,

were also automatically generated from the segmentation process. The automatically

generated 2D fetal brain masks were not optimal for most of the subjects, resulting in over-

and under-estimations of fetal brain tissue in the slices. The false 2D masks would result in

meaningless volumetric reconstruction, therefore quick manual adjustments of the 2D masks,

such as filling and excluding pixels, were performed on all automatic 2D masks.
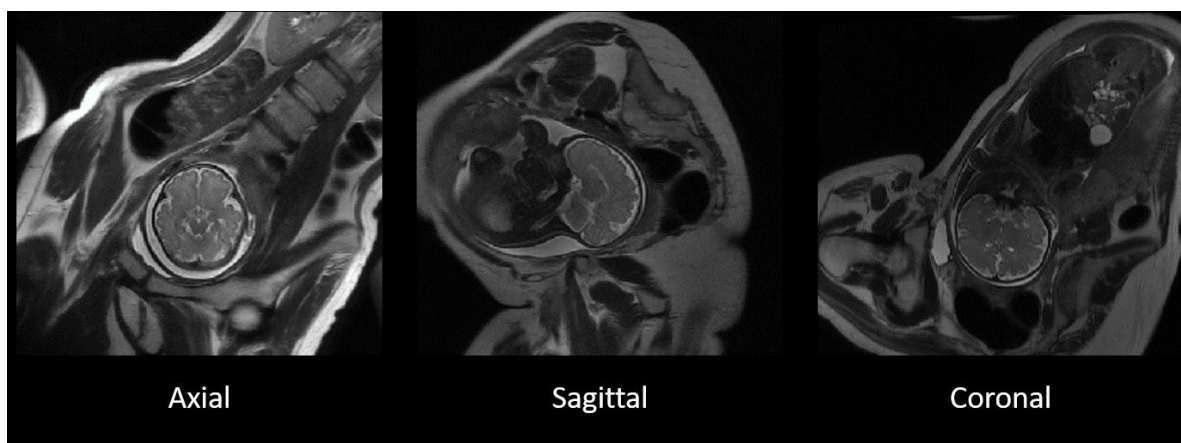
Figure 2-2-2: The original T2-weighted acquisition of a fetal MR image in axial, sagittal, and coronal planes. T2-weighted images acquired separately in three separate image planes in the axial (left), sagittal (middle) and coronal (left) in a representative participant. The three image planes were subsequently used for the reconstruction of three-dimensional images.
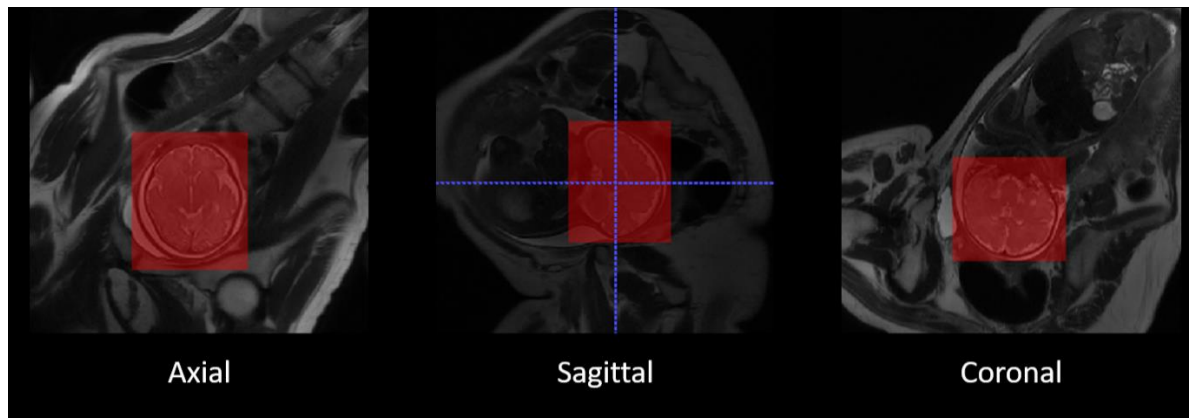
Figure 2-3: The red boxes represent the broad localization of the fetal brain in the three different image planes. T2-weighted images acquired separately in three separate image planes in the axial (left), sagittal (middle) and coronal (left) in a representative participant with broad localization of the fetal brain (red boxes).

After segmenting fetal brains in the 2D planes, the 2D slices were reconstructed into

3D volumes and the 2D fetal brain segmentations were also reconstructed into 3D space. The

2D MR image slices could be corrupted by bias field signals that are low-frequency to blur

the high-frequency contents, such as edges and contours. Intensity variance was also a consequence of existing bias field signals that the same tissue had uniformed pixel gray level in the images. Thus, the segmented 2D fetal brain slices were firstly bias field corrected. Secondly, the bias field corrected 2D slices were reconstructed into 3D volume by the slice-to-volume process that rigidly registered the 2D slices to one randomly selected target slice from the fetal brain MR images so that all the slices were volumetrically aligned. The slice-to-volume process also used linear regression to correct and match the slices voxel intensities to the target slice's voxel intensity. Thirdly, volume-to-volume process was performed on the 2D slices and previously segmented 2D masks to reconstruct into 3D volumes and 3D fetal brain masks in native space. Subsequently, the native-space 3D volumes were then rigidly registered to a spatiotemporal atlas developed from images from typically-developing fetuses to obtain the volumetric reconstruction in the standard anatomical planes of template space.

The NiftyMIC platform offers two automatic frameworks: niftymic_segment_fetal_brains and niftymic_run_reconstruction_pipeline for straightforward command line calls. We used niftymic_segment_fetal_brains for automatic fetal brain segmentation that can generate 2D fetal brain masks and niftymic_run_reconstruction_pipeline for the automatic volumetric reconstruction, including bias field correction, slice-to-volume, and volume-to-volume reconstruction steps that generated 3D fetal brain volumes in standard anatomical planes and corresponding 3D fetal brain masks. These two frameworks both used default parameters for the CNN and morphological processing algorithms.

2.1.6   *Registration-based subcortical segmentation*

The reconstructed 3D fetal brain masks were applied onto the reconstructed 3D brain

volumes for fetal brain skull stripping (Figure 2-4). The 3D brain volumes were segmented

with the binary masks for fetal brain-only MR images, which was a prerequisite for later

subcortical segmentation utilizing image registration since image registration for tissue

alignment assumes the target object and the moving object are the same tissue with similar

shapes. Registering the skull-stripped fetal brain template to subject fetal brain excluding

maternal matters would aid in reducing unrelated contents for meaningful registration result.

The skull stripping step was performed using 3dcalc from AFNI toolkit that multiplied the

reconstructed 3D fetal brain image with the binary 3D masks. Then the orientation tags of the

skull-stripped MR images were manually adjusted according to the orientation age-

appropriate fetal brain template using the ITK-SNAP GUI (graphical user interface).
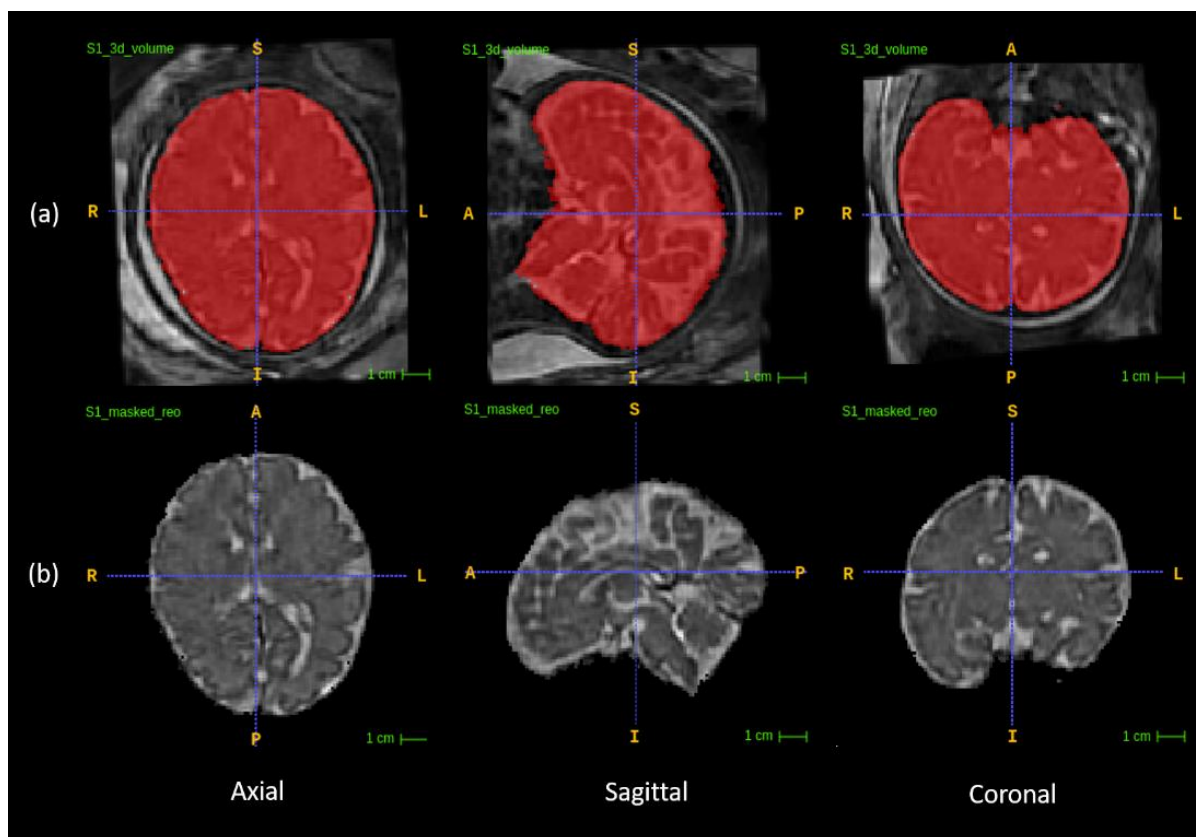
Figure 2-4: Fetal brain segmentation. Row (a) includes the volumetrically reconstructed fetal brains in three planes. The red areas are the manually segmented fetal brain binary masks. Row (b) includes the orientation-corrected and skull-stripped (using the binary masks in red) fetal brain volumes in three planes.

Two different types of automatic registration tools, affine and nonlinear atlas registration algorithms, were applied to the reconstructed images and compared to determine an optimal fetal subcortical segmentation strategy. Nonlinear atlas registration was performed using ANTs (Avants et al., 2008) using the well-known SyN (symmetric image normalization) method (Avants et al., 2008) and linear (affine) atlas registration was performed using FLIRT (Jenkinson et al., 2001 & 2002). The fetal brain atlas (Figure 2-5) is an averaged template from fetuses imaged at 36 weeks gestational age with predefined labels of vital deep brain structures including the thalamus and cerebellum. The atlas was nonlinearly and linearly registered into the native participant 3D MRI space. The

transformation matrix was saved and applied onto the atlas mask to warp the tissue labels

into subject space. The transformed atlas labels were used as thalamus and cerebellum masks

(Figure 2-6) and were compared with manual masks by calculating Dice similarity

coefficients for the reliability test.
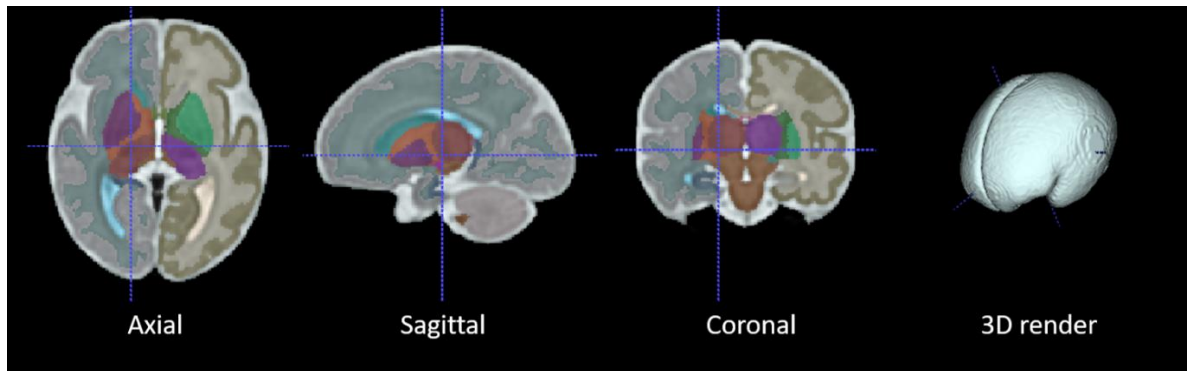
Figure 2-5: The average 36-weeks GA fetal brain template including cerebellum and thalamus labels. The axial, sagittal, coronal, and 3D rendered views of the age-appropriate fetal brain atlas whereby deep brain tissues are colour-coded.
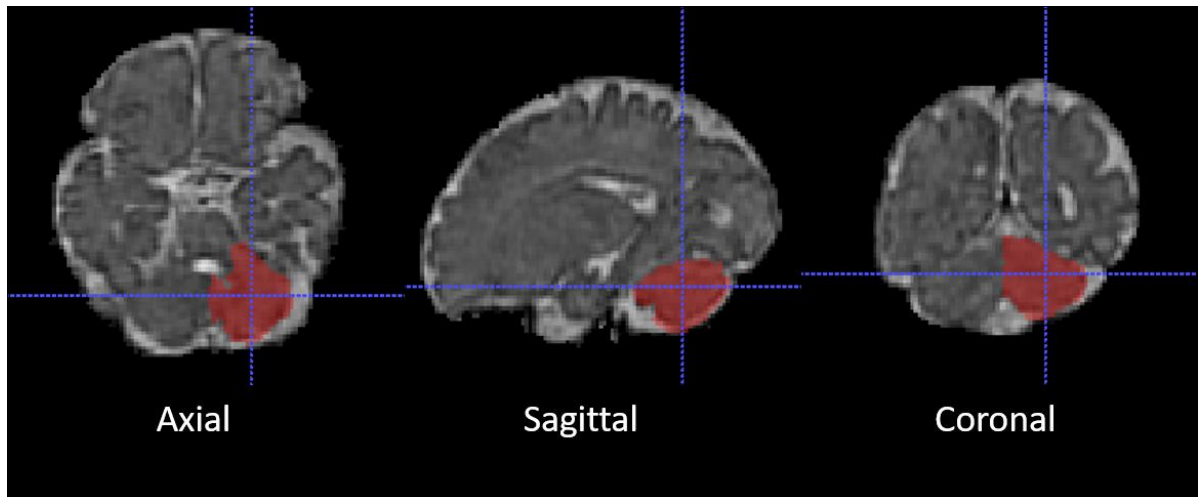
Figure 2-6: The registered template label into the subject space. This figure shows the linearly registered left cerebellum label using ANTs. The reconstructed 3D fetal brain volumes were skull-stripped. The orientations were transformed into the same image orientation of the fetal brain atlas as the original acquisitions of the MRI scans were oriented based on the position of mothers' bodies in the scanner. The manual and automatic cerebellum and thalamus segmentations were then performed on the processed reconstructed 3D volumes.

The applied FLIRT registration tool implemented the correlation ratio similarity metric for

linear (affine) registration as the default parameters. The ANTs registration tool used a

mutual information similarity metric for both linear (rigid and affine) registration and nonlinear (SyN, Symmetric Image Normalization) registration in the antsRegistrationSyNQuick.sh script as the default. Different combinations of similarity metrics for both linear and nonlinear image registration of ANTs were also applied and compared to find the more suitable image registration method for our MR image data. The selected fetal brain template and our acquired fetal brain were both T2-weighted images, in which case the grayscale signals of the same tissue in the target image and the moving image were theoretically similar, where similarity metrics such as cross correlation are beneficial for measuring pixel intensity differences. Hence, the cross-correlation similarity metric that was provided in the ANTs toolbox that is sufficient for intra-modality registration was used for rigid, affine, and SyN registration algorithms. Although the template and the participant images were in the same modality, there existed considerable differences in image intensities in the voxels. The image intensity information of the atlas and that of the MR images from the individual subjects were considerably different. The atlas intensities ranged from 0 to 3484 and the individual subject MR image intensities ranged up to 32767. The mean intensity of non-zero pixels in a random volumetrically reconstructed fetal brain MR image was approximately 11433 and that in the template was approximately 1742. The tissue contour in the atlas had higher contrast compared to that in the individual subject images. In this case, it was worth testing and comparing the impact of using similarity metrics that predict the pixels of interest in the moving image given the pixel intensities in the target image that does not require the tissue boundary signals to be similar. Therefore, mutual information similarity metric provided by the ANTs toolkit was used for all three registrations (rigid, affine, and SyN).

The FLIRT linear image registration was performed using the flirt command line tool with the DOF (degree of freedom) option set at 12. The ANTs linear image registration (12 DOF) was performed using the antsRegistration command line tool by defining the rigid and affine transformations. The ANTs nonlinear registration (millions of DOF) algorithm using the mutual information metric was performed using the provided default antsRegistraionSyNQuick.sh script. Keeping every other parameter the same as antsRegistraionSyNQuick.sh script, the ANTs nonlinear registration using the cross correlation metric was also performed using the antsRegistration command line tool by adding the SyN transformation definition upon the linear registration parameters. To apply the transformation matrices to the atlas masks, the FLIRT command line tool was defined with the applyxfm option and the ANTs command line tool was antsApplyTransformations.

The fetal whole brain volumes and cerebellum and thalamus volumes were computed from the skull-stripped fetal brain masks and the subcortical masks. The command line tool used for this step was fslstats from FSL that outputs the image voxel and tissue volume in unit of mm^3.

2.1.7   Manual subcortical segmentation

Anonymized with respect to gestational age at birth and all other functional outcome measures, the left and right thalamus and cerebellum were delineated in all 10 reconstructed T2-weighted images. The 3D reconstructed T2-weighted images were visualized and segmented using ITK SNAP. The displays provided simultaneous coronal, sagittal and axial views of the brain and created a 3D image of the thalamus and cerebellum. Thalamus and cerebellum masks were created through the visual identification and tracing of these brain regions in each slice. A three-step segmentation protocol was applied to each of the images in order to segment both the cerebella and thalami. The thalamus was segmented first, followed

by the cerebellum. The thalamus was present in approximately 40 slices, whereas the cerebellum was present in approximately 50 slices. Segmentations were based on the intensity differences between the white matter and gray matter.

Step 1: Segmentation of the Cerebellum and Thalamus. Dependent on the participants and the resolution of the images, the rater segmenting the images manually composed segmentations through all three viewpoints (sagittal, coronal and axial) to ensure that the masks were accurate in all viewpoints. The initial segmentations that were completed were verified in the other views and any incorrectly identified areas were omitted and revised.

Step 2: Inspection of the 3D Surface. The segmented cerebellum and thalamus masks were represented in a 3-D display through ITK-SNAP. It is expected that the surface of both the cerebellum and thalamus is smooth throughout, so any areas on the masks that protruded excessively were trimmed through a smoothing feature on ITK-SNAP.

Step 3: Segmentation of Left and Right Hemispheres. Once segmentations were complete, cerebellum and thalami masks were segmented into left and right hemispheres. By identifying the midline of the brain, each mask was segmented and split into the left and right hemispheres. These segmentations were verified across all three viewpoints to ensure accuracy and to revise original segmentations.

2.1.8   *Protocol reliability testing*

Three fetal MR images (33%) were randomly selected and re-segmented by the same rater to assess the reliability of the 3-step manual segmentation protocol. The re-segmentations of both the left and right thalami and cerebelli in the fetal MR images were performed 6 months after the original segmentations to ensure that the rater's memory would not unduly influence

the results. This type of test-retest metric, intra-rater reliability, can be used as an upper

bound metric to assess the accuracy of the segmentations of the thalamus and cerebellum.

The reliability of the protocol was measured using Dice Similarity metric, which evaluates

the spatial and volumetric overlap of the original and re-segmented label volumes.

2.1.9   Manually adjusting automatically generated masks from NiftyMIC

Anonymized with respect to gestational age at birth and all other functional outcome

measures, whole brain masks were manually segmented in all nine fetal brain scans. A three-

step segmentation protocol (described below) was applied to each of the images in order to

segment the whole brain masks. The whole brain was present in approximately 90 slices.

Step 1: Automatic Segmentation. Whole brain masks were generated automatically

for each subject using NiftyMIC software.

Step 2: Manual Segmentation. Brain masks generated automatically through

NiftyMIC were contrasted against the original brain scan for each subject on ITK-SNAP.

Each mask was manually edited to ensure that the mask fit the image. Dependent on the

subject and the clarity of the image, the individual segmenting the images manually worked

through all three viewpoints (sagittal, coronal, and axial) to ensure that the masks were

accurate in all viewpoints. The initial segmentations that were completed were verified in the

other views and any incorrectly identified areas were omitted and revised. Any area of the

mask that protruded excessively outside of the brain region was removed. Additionally, any

areas of the brain that were not covered by the mask were filled in appropriately.

Step 3: Segmentation of Left and Right Hemispheres. Once the segmentations

were complete, the whole brain masks were segmented into left and right hemispheres. By

identifying the midline of the brain, each mask was segmented and split into the

corresponding hemisphere. These segmentations were verified across all three viewpoints to ensure accuracy and to revise the original segmentations.

2.1.10 Statistical analysis

The robustness of the entire automatic fetal deep brain structure segmentation workflow was tested by comparing the automatically segmented masks and manually segmented masks by calculating the Dice Similarity coefficient of the common areas covered. The Dice Similarity coefficient was calculated using the formula $D = \frac{2(A \cap B)}{A+B}$, where A and B represent the automatic mask and the manual mask, that computes the ratio of two times of the common area to the sum of two areas. Statistical analyses were performed using SPSS (version 26, Armonk, NY). The resulting Dice similarity coefficients were non-normally distributed. Therefore, a nonparametric Friedman's test for paired data was applied to the Dice similarity coefficients. An alpha level of $p<0.05$ was selected. According to the typical guidelines of the Dice Similarity coefficients interpretation (Cohen, 1960), this automatic segmentation method is considered reliable when the coefficient is greater than 0.8.

To calculate the Dice similarity coefficients, the regions of interest (ROI): right cerebellum, left cerebellum, right thalamus, and left thalamus were firstly extracted from the registration-based subcortical masks using the combination of 3dcalc and 3dcluster command line tools from AFNI. The reason for this step is that the manually drawn subcortical masks of one subject were traced separately for the four ROI described above. The Dice similarity coefficients were then calculated by overlay the extracted automatic ROI with the corresponding manual ROI using the c3d -overlay command line tool of convert3d package from ITK-SNAP. The c3d command line tool printed the Dice similarity coefficients in

terminal by default that was not ideal for data organization, therefore we redirected the

output numbers to print into text files. Then an in-house Python script was developed to read

and write the Dice similarity coefficients from the text files into csv format.

2.1.11 Software installation and operating system decency

The computer used in this study was built with the 10th generation of intel i7 CPU (central

processing unit) with 8 cores and 16 threads, 32GB of RAM (random access memory). The

operating system used for this study was Ubuntu 18.04. ITK-SNAP (version 3.6.0), AFNI

(version 20.3.01), convert3d package (version 1.0.0), FSL package (version 6.0.4) including

FLIRT was installed locally from source. ANTs was provided by and installed on the SciNet

supercomputer center at the University of Toronto (i.e., Compute Canada). NiftyMIC was

installed with the provided Docker image.

3   Chapter Three

3.1   Results

3.1.1   2D fetal brain segmentation and 3D volumetric reconstruction

The 2D fetal brain masks of the stacks of the original fetal brain MR images were

automatically segmented using NiftyMIC in the axial, coronal, and sagittal image planes. For

the NiftyMIC volumetric reconstruction algorithm to perform optimally, the 2D auto-masks

were manually adjusted using ITK-SNAP for the over- and under-estimations of fetal brain

tissue by the NiftyMIC segmentation algorithm. The volumetric reconstruction process was

performed on all nine subjects. Eight 2D masks (89%) were successfully reconstructed into

3D space (Figure 3-1), and one participant's data (ID 2) was rejected due to a complete

failure of the fetal brain segmentation and volumetric reconstruction routine.
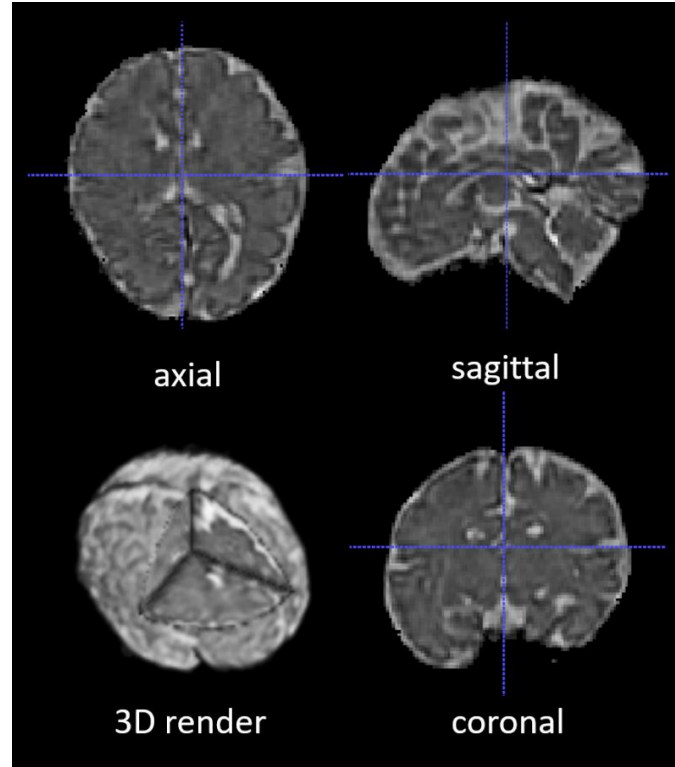
Figure 3-1: Segmented and volumetrically reconstructed fetal brain image using NiftyMIC. The original 2D slices of fetal MR images were automatically segmented and manually adjusted for fetal brain 2D masks. Then the 2D slices and 2D brain masks were reconstructed into 3D volumes and 3D masks with motion correction. This figure shows and example of the skull-stripped, orientation-adjusted 3D fetal brain volumes in axial, sagittal, coronal, and 3D rendered views.

Skull stripping and orientation tags correction were successfully applied on the reconstructed 3D volumes. Based on the skull-stripped automatically reconstructed 3D fetal brain MR images, manual segmentations of thalamus and cerebellum on both left and right sides were successfully performed. The median volumes of the subcortical regions of interest and whole brain volumes are presented in Table 3-1 along with the interquartile ranges (IQR).

Table 3-1: Fetal brain volumes

Characteristic	Total (n=8)
Cerebellum, Median volumes mm^3 (IQR)	14756 (14373-17794)
Thalamus, Median volumes mm^3 (IQR)	5907 (4952-6994)
Whole Brain, Median volumes mm^3 (IQR)	410224 (386297-464227)
GA, Median weeks, (IQR)	36.6 (36.1-37.3)

Gestational age (weeks), IQR, interquartile range (25%ile-75%ile)

The volumes of the averaged left and right thalamus and cerebellum were plotted against gestational age (Figure 3-2). Both the cerebellum (r=0.7, p=0.035) and the total cerebral volumes (r=0.8, p=0.01) were positively associated with gestational age, indicative of larger volumes at older gestational ages. The thalamus showed no association with gestational age (r=-.1, p=0.7).
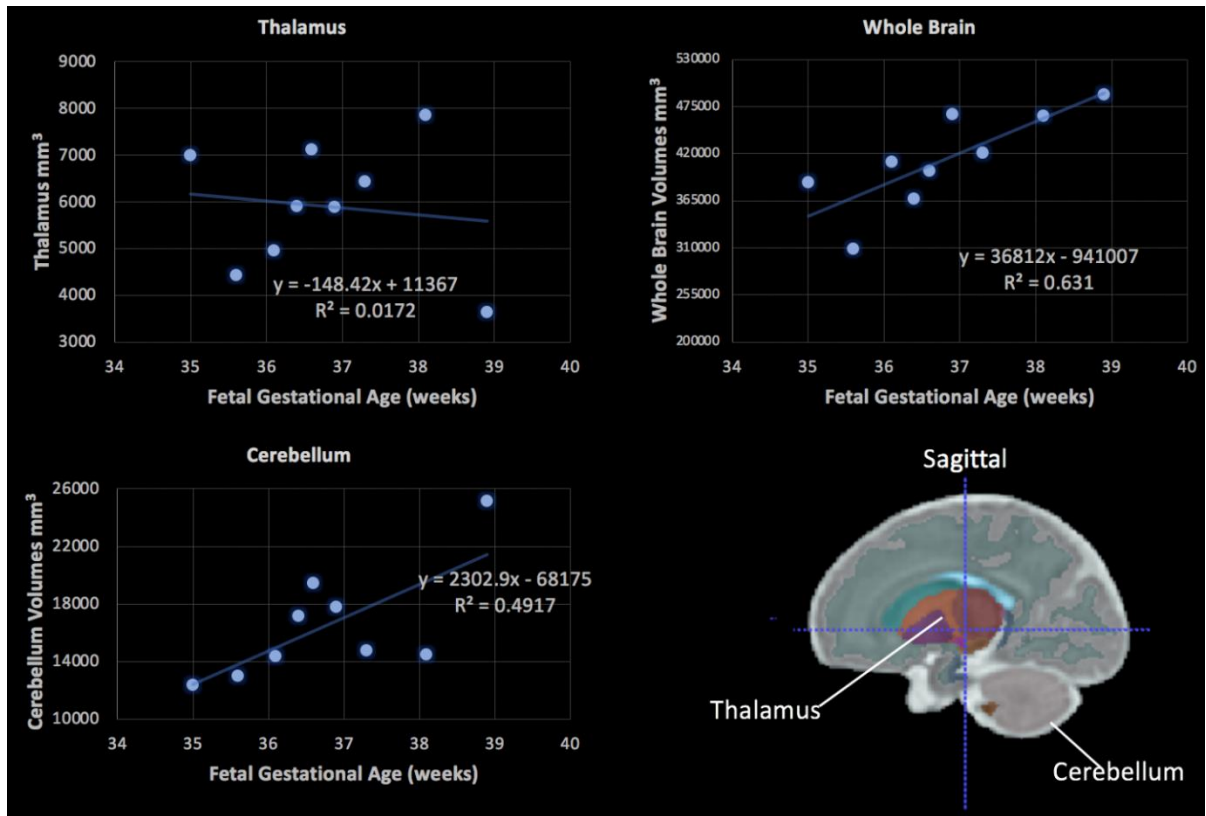
Figure 3-2: Fetal volumes (y-axis) plotted in relation to gestational age (x-axis). Fetal thalamus (top, left), whole brain (top, right) and cerebellum (bottom, left) volumes plotted in relation to gestational age in weeks. The cerebellum and total cerebral volumes showed a positive linear association with gestational age (both, p<0.05). (Bottom, right) The colour-coded fetal atlas overlaid on a template MRI demonstrating the location of the thalamus (orang/purple) and the cerebellum (grey).

3.1.2   Manual segmentation protocol validation: intra-reliability test

Three (37.5%) fetal images were randomly selected from the 8 processed participants. The

thalamus and cerebellum were re-segmented to assess the consistency of the 3-step manual

segmentation protocol. Re-segmentations of both the left and right thalami and cerebelli in

these images were performed at least 6 months after the original segmentations were

performed. The intra-reliability test results were listed in Table 3-2. The IQR of the median

Dice similarity coefficients of cerebellar and thalamic segmentations were 0.83 and 0.68

respectively. The overall median Dice similarity coefficients was approximately 0.77.

Table 3-2: Intra-reliability test – Dice similarity coefficients

	Dice Similarity Coefficients
Cerebellum	0.83 (0.83-0.83)
Thalamus	0.68 (0.67-0.70)
Overall	0.77 (0.68-0.83)

The median Dice similarity coefficients for cerebellum segmentation, thalamus segmentation, and both segmentations combined. IQR, interquartile range (25%ile-75%ile)

3.1.3 *Registration-based segmentation reliability test: comparisons of Dice similarity coefficients*

The nonlinear and linear registrations of the 36-week GA fetal brain atlas into the native spaces of the individual fetal MR images were successfully processed using FLIRT and ANTs. The median Dice similarity coefficients comparing the five image registration methods to the manual segmentation method, which were: (1) FLIRT linear registration (affine) using the correlation ratio similarity metric, (2) ANTs linear registration (rigid and affine) using the mutual information (MI) similarity metric (ANTs Lin MI), (3) ANTs linear registration using the cross-correlation (CC) similarity metric (ANTs Lin CC), (4) ANTs nonlinear registration (rigid, affine, and SyN) using the MI similarity metric (ANTs NL MI), and (5) ANTs nonlinear registration using the CC similarity metric (ANTs NL CC) for left and right cerebellum and thalamus segmentations were listed in Figure 3-4 to Figure 3-7. The left-sided cerebellar masks produced by the five registration methods using different similarity metrics were shown in Figure 3-3.
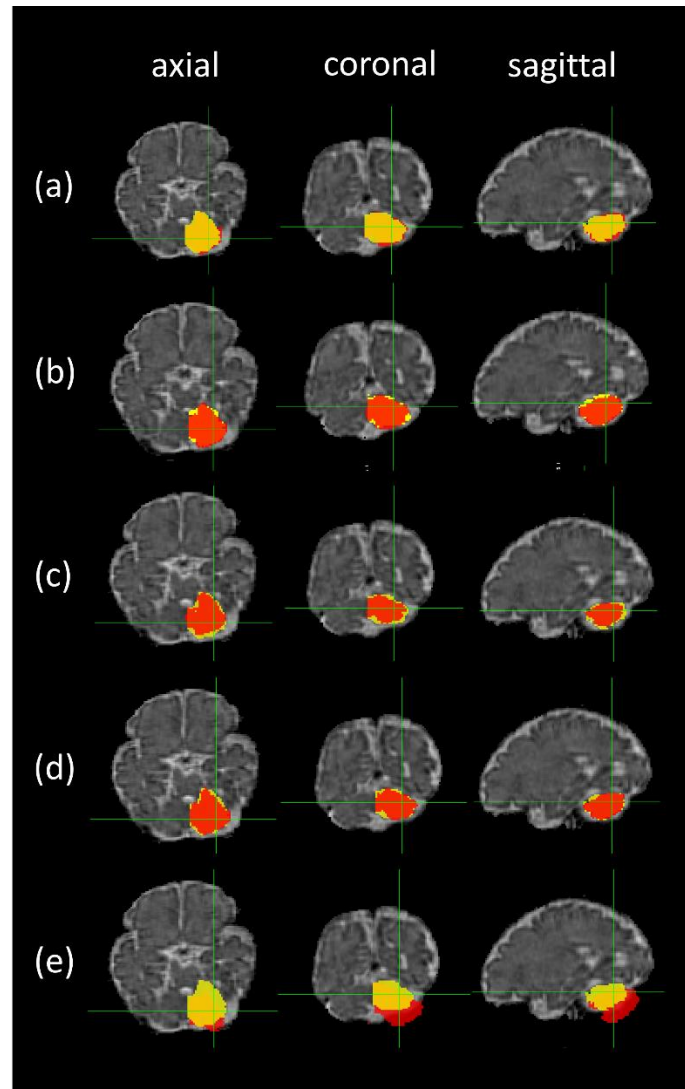
Figure 3-3: Left cerebellar masks: registration-based segmentation (red) vs manual segmentation (yellow). The masks are shown in axial, coronal, and sagittal planes from left to right. Row (a) ANTs linear registration (MI); (b) ANTs linear registration (CC); (c) ANTs nonlinear registration (CC); (d) ANTs nonlinear registration (MI); (e) FLIRT linear registration.

The median Dice similarity coefficients of the five registration methods for the cerebellum segmentation, thalamus segmentation, and both segmentations were listed in Table 3-2. Overall, the FLIRT linear registration resulted in non-optimal estimation with gross misalignment of the masks on the fetal MR image. Overall, the ANTs linear registration (CC) had the highest median Dice Similarity index, and ANTs linear registration

(MI) had nearly identical performance. The ANTs nonlinear registration (MI and CC) had

comparable results.
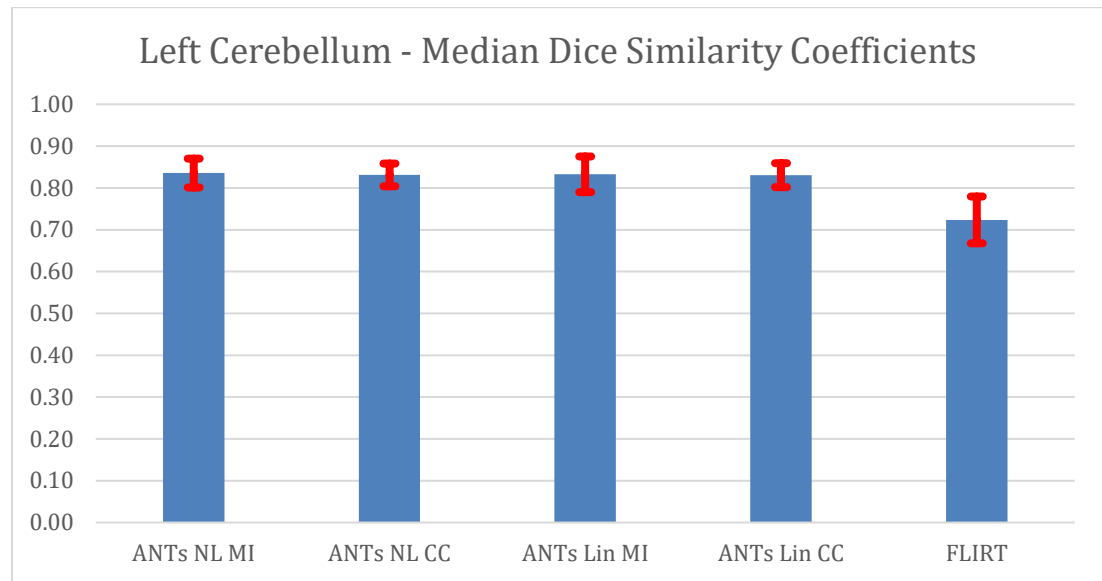
Figure 3-4: Median Dice similarity coefficients of the left cerebellum segmentations using 5 methods. The ANTs-based registration methods produced similar results while the FLIRT registration produced the lowest Dice Similarity value. Error bars are the interquartile ranges (25th%ile-75th%ile).
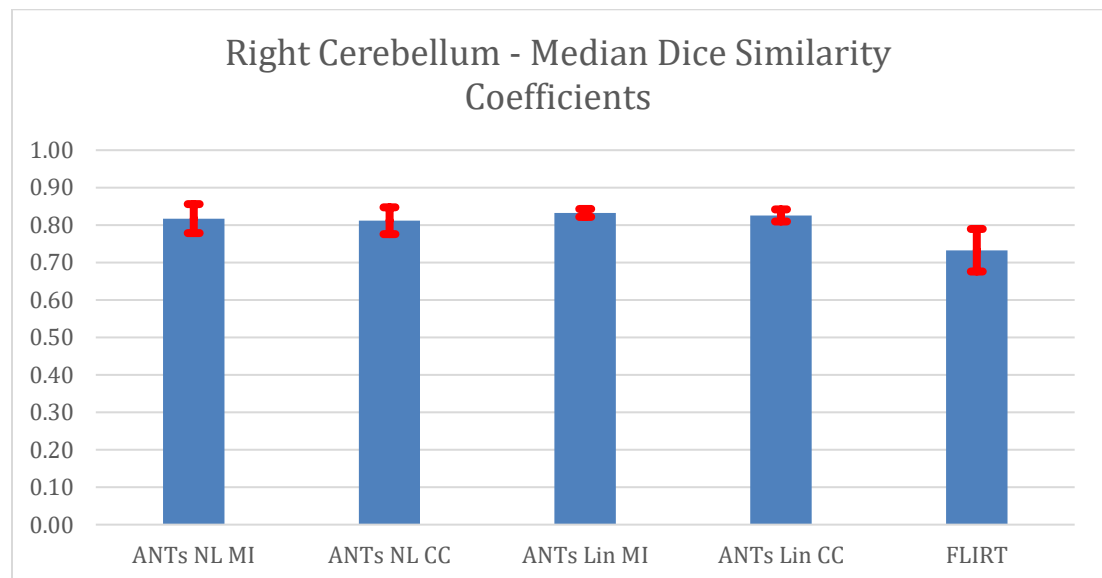
Figure 3-5: Median Dice similarity coefficients of the right cerebellum segmentations using 5 methods. ANTs Lin MI and CC produced the highest Dice similarity coefficients while the ANTs nonlinear registration had comparable results. FLIRT registration had the lowest Dice Similarity value. Error bars are the interquartile ranges (25th%ile-75th%ile).
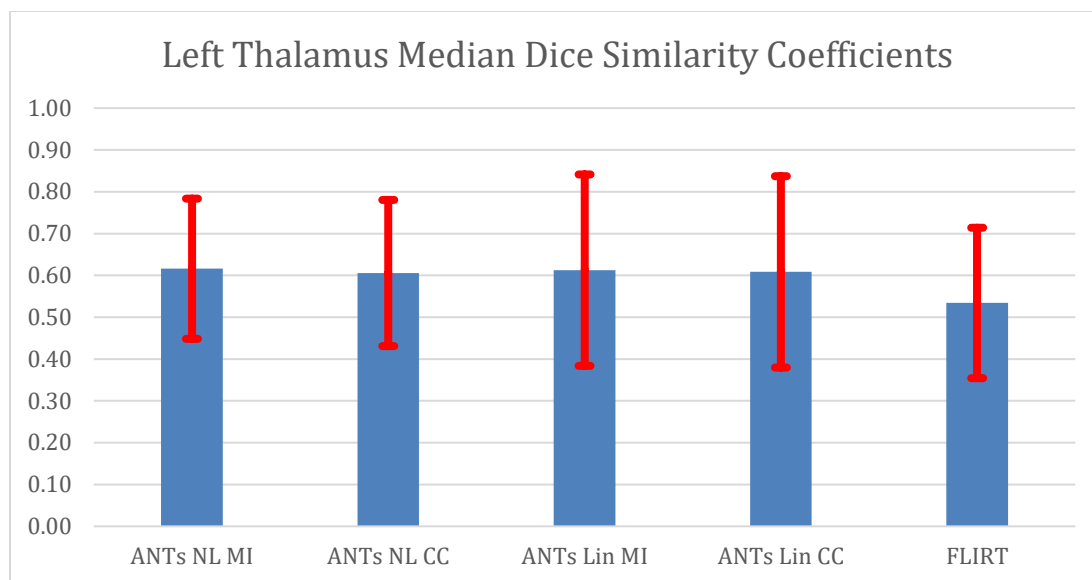
Figure 3-6: Median Dice similarity coefficients of the left thalamus segmentations using 5 methods. The median Dice similarity coefficients of thalamus segmentations were lower with higher IQR than that of cerebellum segmentations of all 5 registration methods. For left thalamus segmentations, the Dice similarity coefficients of ANTs-based registration methods were similar and higher than that of FLIRT registration. Error bars are the interquartile ranges (25th%ile-75th%ile).
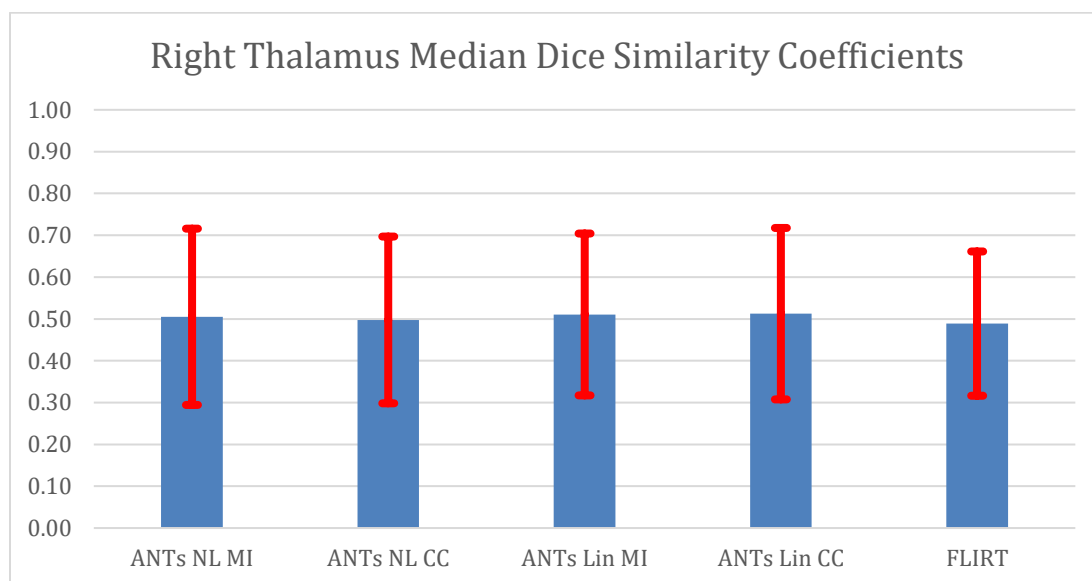
Figure 3-7: Median Dice similarity coefficients of the right thalamus segmentations using 5 methods. For right thalamus segmentations, the Dice similarity coefficients were comparable for all 5 registration methods while FLIRT produced sub 0.5 Dice Similarity value. Error bars are the interquartile ranges (25th%ile-75th%ile).

Table 3-3: Median Dice Similarity Coefficients

Registration Method	Both	Cerebellum	Thalamus
ANTs Lin CC	0.78	0.83	0.55
ANTs Lin MI	0.79	0.83	0.56
ANTs NL MI	0.75	0.83	0.56
ANTs NL CC	0.76	0.82	0.54
FLIRT	0.66	0.73	0.52

The median Dice Similarity coefficients of cerebellum, thalamus, and both subcortical segmentations using 5 registration methods.

The median Dice similarity coefficients of both subcortical segmentations revealed that ANTs Lin CC and MI were the highest while the nonlinear registrations were comparable while the FLIRT was the lowest. The Dice similarity coefficients for the linear (i.e., ANTs rigid and affine, and FLIRT affine) and nonlinear (i.e., ANTs nonlinear with MI and CC similarity metrics) methods for the thalamus and cerebellum segmentations were compared using Friedman's tests. The cerebellar Dice similarity coefficients were compared and were significantly different from one another (Figure 3-8, n=16, df=4, test statistic=38.75, $p<0.001$).
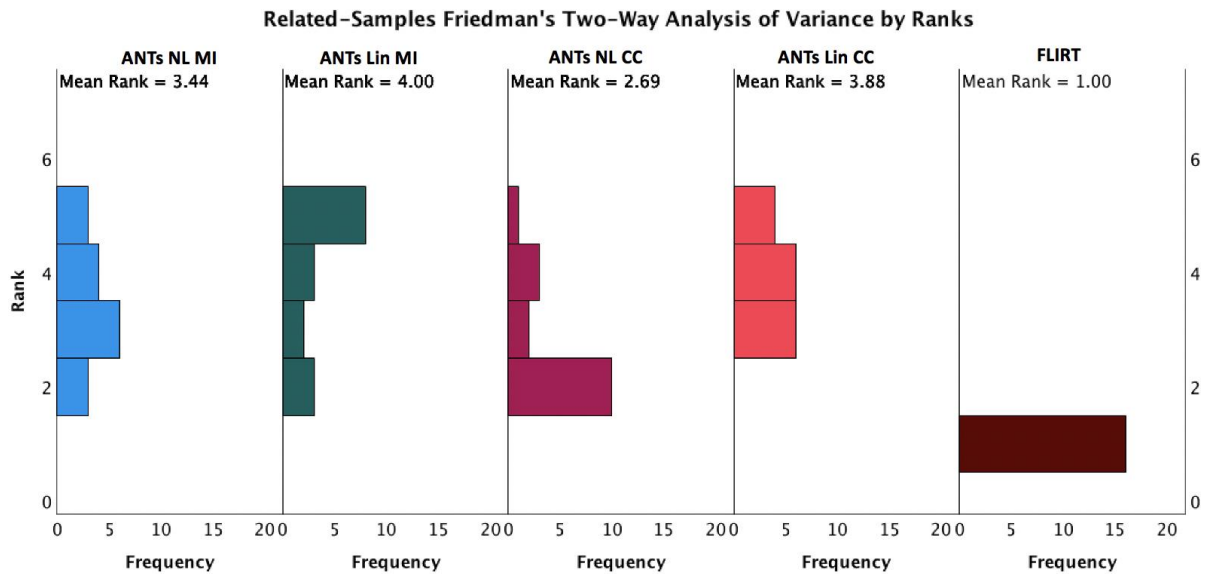
Figure 3-8. Results of a Friedman's test comparing the Dice similarity coefficients amongst linear and nonlinear registration algorithms for the fetal cerebellum segmentations. The Friedman's test of cerebellum segmentations indicated that the ANTs Lin MI (blue) and CC (coral) had the highest rank among all methods while the FLIRT registration methods (brown) had the lowest rank. Both ANTs linear registration methods had the lowest variance from the manual segmentation and FLIRT had the highest variance.

Table 3-4: Post hoc comparisons: Dice similarity coefficients for the fetal cerebellar segmentations.

Sample 1-Sample 2	Std. Test Statistic	p value*
FLIRT - ANTs NL CC	3.02	**0.025**
FLIRT - ANTs NL MI	4.36	**<0.001**
FLIRT - ANTs Lin CC	5.14	**<0.001**
FLIRT - ANTs Lin MI	5.37	**<0.001**
ANTs NL CC - ANTs NL MI	1.34	0.99
ANTs NL CC - ANTs Lin CC	-2.12	0.336
ANTs NL CC - ANTs Lin MI	2.35	0.189
ANTs NL MI - ANTs Lin CC	-0.78	0.99
ANTS NL MI - ANTs Lin MI	-1.01	0.99
ANTs Lin CC - ANTs Lin MI	0.22	0.99

Results of a Dunn's pairwise post hoc tests on the Dice similarity coefficients. A Dunn's test for post hoc testing revealed that the ANTs-based registration algorithms outperformed the FLIRT linear registration algorithm (all, p<0.05). The ANTs Lin CC registration algorithm on the cerebellum segmentations performed the best while all other ANTs-based registration algorithms demonstrated comparable performance to the ANTs Lin CC registration algorithm (p=0.99). *Bonferroni corrected for multiple comparisons

Subsequently, the Dice similarity coefficients produces by the linear and nonlinear

registrations algorithms compared to the manual segmentations, were examined for the

thalamic segmentations and were also found to be significantly different (Figure 3-9, n=16,

df=4, test statistic=19.55, p<0.001).
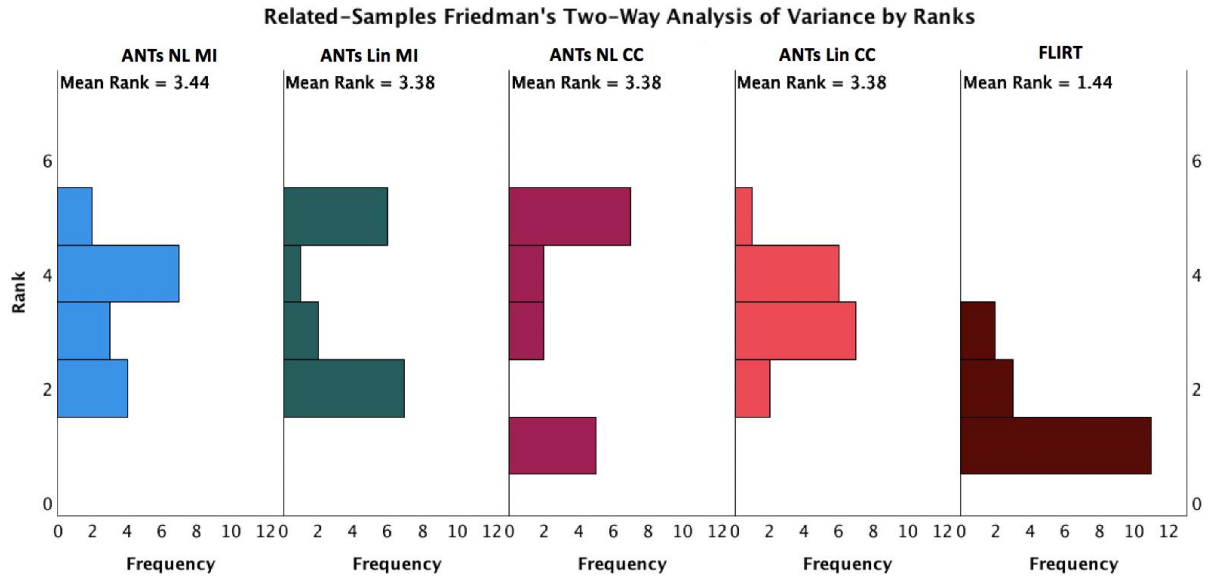
Figure 3-9. Results of a Friedman's test examining the Dice similarity coefficients amongst affine and nonlinear registration values for the fetal thalamus segmentations. The Friedman's test of thalamus indicated that the ANTs-based linear and nonlinear registrations had similar ranks, which were significantly higher than that of the FLIRT registration methods. This revealed that ANTs-based registration methods generally had notable higher agreement with manual segmentation results than the FLIRT registration method.

Table 3-5: Post hoc comparisons: Dice Similarity Coefficients for the fetal thalamic segmentations.

Sample 1-Sample 2	Std. Test Statistic	p value*
FLIRT - ANTs NL CC	3.47	**0.005**
FLIRT - ANTs NL MI	3.47	**0.005**
FLIRT - ANTs Lin CC	3.47	**0.005**
FLIRT - ANTs Lin MI	3.58	**0.003**
ANTs NL CC - ANTs NL MI	0.00	0.99
ANTs NL CC - ANTs Lin CC	0.11	0.99
ANTs NL CC - ANTs Lin MI	0.11	0.99
ANTs NL MI - ANTs Lin CC	0.00	0.99
ANTS NL MI - ANTs Lin MI	0.11	0.99
ANTs Lin CC - ANTs Lin MI	0.00	0.99

Results of a Dunn's pairwise post hoc tests on the Dice similarity coefficients post-hoc testing revealed that the Dice similarity coefficients affine-based FLIRT transformations were significantly lower than those calculated using ANTs (all, $p<0.05$). Additionally, no statistically significant differences in the Dice similarity coefficients for the ANTs-based linear and nonlinear registration algorithms were evident. *Bonferroni corrected for multiple comparisons.

3.1.4   *Atlas-based segmentation of the fetal brain: subcortical volumes*

The fetal atlas was linearly registered to the individual 3D reconstructed images using ANTs

Lin MI. The subcortical volumes were extracted and plotted in relation to gestational age.

The volumes of the amygdala, caudate nucleus, putamen, globus pallidus and hippocampus

are plotted in relation to gestational age in Figure 3-10. Overall, each brain structure showed

a positive linear association with age; however, none of the brain regions were significantly

associated with age (all, $p>0.05$) based on bivariate correlations. The results were maintained

when adjusting for total cerebral volumes.
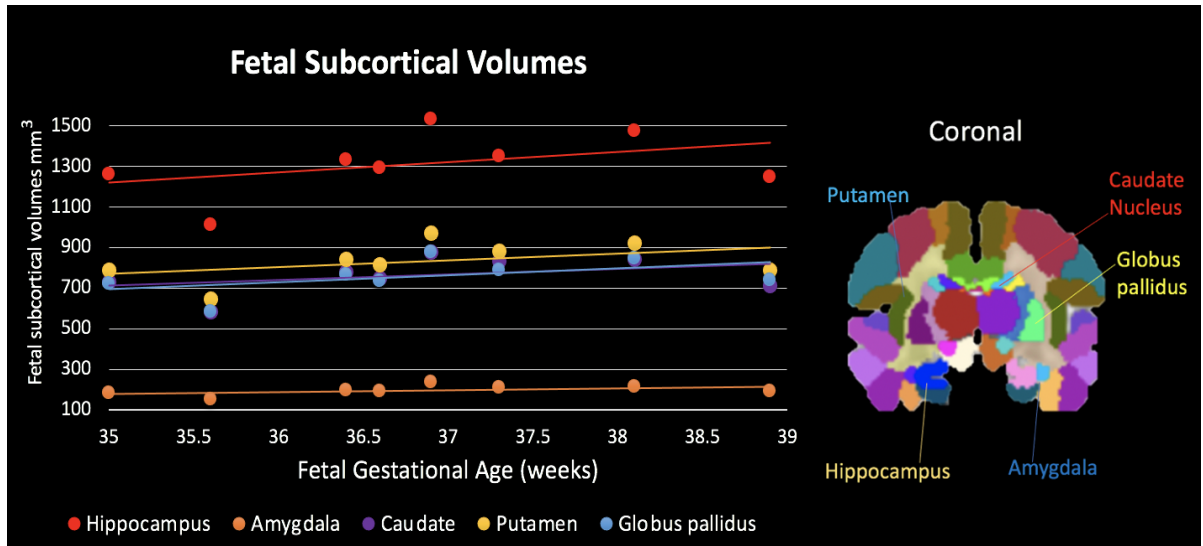
Figure 3-10. Atlas-based subcortical volumes (y-axis) plotted in relation to gestational age (x-axis). The volumes for the amygdala, caudate nucleus, putamen, globus pallidus, and hippocampus all demonstrated a non-significant linear association with fetal GA (all, p>0.05).

4   Chapter 4

4.1   Conclusions and future directions

Fetal MRI represents one of the next frontiers in clinical, translational and basic science research, not only to improve our understanding of the developing fetal brain, but to aid in early diagnosis, particularly for fetuses who are at-risk for adverse neurodevelopmental outcomes. The study of the brain and other organs in the fetus has been limited to primarily non-invasive ultrasound technology. While ultrasound offers many advantages due to its low cost and ease of use in hospital settings, it is limited in terms of its spatial resolution to study fetal brain structure. MRI of the fetal brain offers superior 3D image resolution and can be used to study brain volumetric development. The goal of this thesis was to develop a semi-automatic pipeline to segment fetal brain volumes acquired in third trimester images. A recently developed deep learning algorithm to mask the fetal brain and reconstruct MR images in second trimester fetuses was employed. Analyzing fetal MR images using typical brain segmentation toolkits designed for adult populations is impractical due to the presence of motion artifacts from fetal movements.

This study aimed to overcome this obstacle in fetal MRI by applying segmentation, volumetric reconstruction, and image normalization toolkits to build a semi-automated process for fetal brain subcortical segmentation in T2-weighted fetal MR images that were acquired during the third trimester of pregnancy. In the first step, the fetal brain was masked in three anatomical 2D planes (axial, sagittal, and coronal planes). Then the segmented 2D fetal brains and brain masks in three planes were reconstructed into 3D brain volumes and masks. After skull-stripping and orientation tag correction, linear and nonlinear image registration methods were evaluated in terms of their accuracy in segmenting cortical and subcortical structures by applying an age-appropriate MRI atlas. In turn, the subcortical

labels of the chosen template were aligned with the individual fetal MR images using two different image registration toolkits (ANTs, FLIRT) using linear (ANTs Lin MI/CC, FLIRT) and nonlinear registration methods (ANTs NL MI/CC). The optimal cortical and subcortical segmentation performance was determined by applying and comparing two image registration toolkits for both nonlinear and linear image registration algorithms with different configurations of similarity metrics. The aligned subcortical labels were then compared with manually segmented subcortical masks of the thalamus and cerebellum. The manually labeled masks were considered as ground truth for later comparison with the atlas-based registration. A linear registration method (ANTs Lin MI/CC) provided improved results compared to a linear transformation (FLIRT). The ANTs MI and CC similarity metrics are optimized in terms of translation, rotation, scaling and shearing during registration of the images. Nonlinear registration methods, while computationally more intensive, may be more suitable for small samples of fetal brain images acquired during the third-trimester in order to have higher quality results. However, overall our findings indicated that linear registration methods using the CC similarity metric performed adequately and may be more practical for processing larger datasets to reduce computational processing time.

4.1.1   *Semi-automatic registration-based fetal subcortical segmentation*

This research utilized machine learning-based segmentation algorithm from NiftyMIC toolkit (Ebner et al., 2020) to significantly mitigate motion artifacts, to segment the fetal brain images acquired during the third trimester in 2D, and to reconstruct 2D images in three planes into 3D volumes. The NiftyMIC toolkit is an open-source toolkit, Python-based software for research within the Guided Instrumentation for Fetal Therapy and Surgery (GIFT-Surg) project, which is an international research consortium focussed on developing technology, tools and training to facilitate fetal surgery (Joyeux et al., 2018). The software

can reconstruct an isotropic, high-resolution brain volume from multiple low-resolution 2D image slices acquired in fetuses. The NiftyMIC 2D segmentation that was originally trained and developed for second-trimester fetal MR images. However, in the current study, when NiftyMIC was applied to third trimester images, and only 8 of the 9 fetal brains were estimated reliably, demonstrating reasonable performance. This masking step is essential for the remaining work-flow steps. Each fetal mask required visual inspected and manual editing to aid in performance of the automatically generated labels. With the adequate 2D fetal brain masks serving as input, NiftyMIC volumetric reconstruction process performed smoothly. Of note, the one fetal scan that NiftyMIC segmented accurately without need for further manual segmentation was from a fetus who was diagnosed growth restriction. In turn, the immaturity of the fetal brain in this particular participant may have contributed to the performance of the NiftyMIC algorithm. The algorithm was designed for less mature fetal brain images acquired in the second trimester. As only one mother with a fetus with growth restriction was recruited to our study, it is not possible to evaluate whether the immaturity of the cortex contributed to the results and further studies with larger samples of growth appropriate and growth restricted fetal MRI scans are needed. Overall, NiftyMIC performed well on the majority of the images and the performance was comparable to what was previously published in second trimester images.

The linear registration algorithms and nonlinear registration algorithms paired with various similarity metrics were successfully applied to register the labeled atlas into native space for cortical and subcortical segmentation of the MRI scans acquired in third-trimester fetuses. The use of different similarity metrics applied to fetal deep-brain segmentation was explored. The registered thalamic and cerebellar masks were compared to manually segmented masks. The ANTs linear registration tool using either the mutual information or

the cross-correlation similarity metric reliably segmented deep brain structures of fetal brains on MR images. The Dice similarity coefficients of ANTs Lin CC indicated a strong agreement between the atlas-based segmentations and the manual segmentations. The ANTs Lin MI registration had nearly identical Dice similarity coefficients for both thalamic and cerebellar segmentations. According to the guidelines for the interpretation of Dice Similarity coefficients (Cohen, 1960), the median Dice Similarity coefficients of ANTs Lin MI and CC indicated a substantial agreement between the registration-based semi-automatic segmentation and manual segmentation for estimating fetal deep brain structures. However, there was a notable performance difference between thalamic and cerebellar segmentations using all five registration methods. The median Dice similarity coefficients of the thalamic segmentations were lower than that of the cerebellar segmentations, which indicated excellent agreement (>0.8) and an only moderate agreement (0.5~0.6) between the registration-based and manual thalamic segmentations using ANTs Lin MI and CC. Findings indicated that ANTs-based nonlinear image registration did not outperform ANTs-based linear image registration for segmenting fetal deep brain structures. ANTs-based linear image registration outperformed the linear transformation in FLIRT. The cross-correlation similarity metric, suitable for intra-modality MR image normalization, was sufficient for our fetal MRI data. The additional calculations involving histogram matching from the mutual information metric did not substantially improve the image registration quality. Therefore, using the cross-correlation metric, that required less computation time to register the data, is sufficient for processing datasets with larger sample sizes.

4.1.2   *Limitations and future improvements*

Machine learning algorithms are known to theoretically perform well to learn and predict data patterns when the process is trained with enough data. This is dependent on the

complexity of the problem and the sophistication of the machine learning algorithm. The NiftyMIC 2D brain segmentation of third trimester fetal MR images specifically did not perform reliably. The NiftyMIC (niftymic_segment_fetal_brains) machine learning algorithm was originally trained with MR images of second-trimester healthy fetuses and fetuses diagnosed with spina bifida. Exponential growth of the fetal brain from the second to the third trimester results in significant cortical and subcortical morphology changes. Additionally, during the third trimester the fetal brain becomes increasingly myelinated. Structural MR images weighted by T1 or T2 relaxation times have different water and fat content in the fetal brain compared to that seen in adults. This results in different signal intensities in the voxels of MR images of the fetal brain, which can vary in fetuses even compared to 6-month infants due to the rapid changes in both overall growth as well as myelination changes (Dubois et al., 2014). Less is known about tissue intensity changes between second trimester and third trimester fetuses; however, in relation to the current work the image intensity of the voxels of the grey and white matter tissues of the training data used for NiftyMIC may have been quite different from that of our third-trimester data. These factors could have notably influenced the machine learning algorithm's performance. Overall, each segmentation and fetal mask produced by NiftyMIC needed to be visually inspected and sometimes manually edited. However, 8 of the 9 images that were tested were able to be segmented and reconstructed using NiftyMIC, indicating comparable performance to that published in second trimester images.

During this study, it has been challenging to acquire data from many patients due to the COVID-19 pandemic restrictions. From March 2020 till August 2021, we were limited to recruit only Western University staff and students at the University scanning site. Thus, we had minimal training data to re-train the NiftyMIC machine learning algorithm for 2D fetal

brain segmentation. Having more data would be ideal to construct a fully automatic pipeline. Recruitment and scanning of participants is still ongoing and more data will offer the opportunity to re-train the machine learning model and automate the 2D fetal brain segmentation processes. On a larger dataset, the performance test of the fetal brain segmentation and the registration-based subcortical segmentation can be more accurately assessed.

Among all five configurations of linear and nonlinear image registration methods, overall, the atlas-based cerebellar segmentations were notably more accurate, compared to the gold-standard manual segmentations, compared to thalamic segmentations using the same methods. The Dice similarity coefficients for thalamic segmentations using ANTs Lin MI and CC were in the moderate range (e.g., 0.5-0.6) while that for the cerebellar segmentations was in the excellent range (e.g., 0.8-0.9). This outcome reflects lower agreement between the fetal brain atlas and the manual rater. The intra-rater reliability was assessed, and the re-segmented labels were found to show good overlap with the original segmentations. However, the over- or under-estimations that may have occurred during our manual segmentation protocol against the atlas was not specifically assessed in this study.

4.1.3   *Implications*

This semi-automatic fetal subcortical segmentation method may be very beneficial for future studies of fetal neurodevelopment. The *in-utero* origin of neurodevelopmental delay reflected in smaller cortical and subcortical volumes can be studied by applying this methodology to a larger fetal MR image dataset that has the potential for significant savings in terms of time and labour devoted to manual segmentations. The whole brain volume and deep brain structures such as the hippocampus are important for learning and memory processes and can be segmented from the MR images for comparison, analysis and developmental outcome

prediction. The proposed methodology could also be utilized for the study of second trimester fetal volumetric development. The fetal neurodevelopment from the second to third trimester could be monitored by segmenting and calculating subcortical and brain growth of in high-risk groups. This method could potentially reveal when the variations in brain morphology occurs to aid in the early diagnosis of fetal brain abnormalities in clinical settings.

ANTs-based linear image registration performed slightly better than ANTS-based nonlinear image registration for aligning the fetal brain atlas to the native MR image space of our dataset. However, this difference was not evident statistically. The amount of deformation of the image when warping the atlas might have been minimal given that the difference in the shape of the fetal brain of the atlas and our acquired fetal MR images was comparable in terms of the anatomy. Linear mis-localization of the fetal brains between the atlas image and the target image contributed to spatial differences. As a result, linear transformations of the atlas fetal brain with only few degrees of freedom resulted in a substantial result compared to nonlinear transformation which utilizes millions of degrees of freedom. The ANTs based linear registration is less time-consuming than nonlinear registration with lower requirement of computation abilities while providing reliable subcortical segmentation performance. Thus, a linear registration method may be more applicable for processing fetal brain MR images when processing large dataset.

4.1.4 Conclusions

Antenatal development of the fetal cortex and subcortical structures is a complex neurophysiological process. The development of the nervous occurs through genetically predetermined events including cellular proliferation, neuronal migration, and differentiation of cells into specialized subtypes followed by synaptogenesis that provides the formation of

cortical and subcortical circuitry. Environmental influences such as maternal diet and even stress can alter these processes and in more severe cases can led to growth restriction of the fetus. The study of fetal brain development using volumetric MRI provides a window into the development of the cortex and subcortical structures in both typical and atypically developing fetuses. In this work, a semi-automatic pipeline to segment the cortex and subcortical structures in third trimester images was developed and evaluated. A novel deep learning-based algorithm was used to segment and reconstruct 3D MR images of the entire fetal brain. An atlas to segment cortical and subcortical structures was aligned to the fetal brain images. Five registration algorithms were evaluated and compared to gold-standard manual segmentations of subcortical structures.

Overall a linear registration algorithm using cross correlation metric provided optimal performance to segment the cortical structures, but a linear registration method provided comparable results and may be favourable to for large datasets or for use in low resource settings without access to high throughput computational facilities.

References

Alom, M. Z., Yakopcic, C., Hasan, M., Taha, T. M., & Asari, V. K. (2019). Recurrent residual U-Net for medical image segmentation. *J Med Imaging (Bellingham)*, *6*(1), 014006. https://doi.org/10.1117/1.JMI.6.1.014006

Avants, B. B., Epstein, C. L., Grossman, M., & Gee, J. C. (2008). Symmetric diffeomorphic image registration with cross-correlation: evaluating automated labeling of elderly and neurodegenerative brain. *Med Image Anal*, *12*(1), 26-41. https://doi.org/10.1016/j.media.2007.06.004

Banović, V., Škrablin, S., Banović, M., Radoš, M., Gverić-Ahmetašević, S., & Babić, I. (2014). Fetal brain magnetic resonance imaging and long-term neurodevelopmental impairment. *Int J Gynaecol Obstet*, *125*(3), 237-240. https://doi.org/10.1016/j.ijgo.2013.12.007

Barkhuizen, M., Abella, R., Vles, J. S. H., Zimmermann, L. J. I., Gazzolo, D., & Gavilanes, A. W. D. (2021). Antenatal and Perioperative Mechanisms of Global Neurological Injury in Congenital Heart Disease. *Pediatr Cardiol*, *42*(1), 1-18. https://doi.org/10.1007/s00246-020-02440-w

Beversdorf, D. Q., Manning, S. E., Hillier, A., Anderson, S. L., Nordgren, R. E., Walters, S. E., . . . Bauman, M. L. (2005). Timing of prenatal stressors and autism. *J Autism Dev Disord*, *35*(4), 471-478. https://doi.org/10.1007/s10803-005-5037-8

Black, M. M., Walker, S. P., Fernald, L. C. H., Andersen, C. T., DiGirolamo, A. M., Lu, C., . . . Committee, L. E. C. D. S. S. (2017). Early childhood development coming of age: science through the life course. *Lancet*, *389*(10064), 77-90. https://doi.org/10.1016/S0140-6736(16)31389-7

Boardman, J. P., Craven, C., Valappil, S., Counsell, S. J., Dyet, L. E., Rueckert, D., . . . Edwards, A. D. (2010). A common neonatal image phenotype predicts adverse neurodevelopmental outcome in children born preterm. *Neuroimage*, *52*(2), 409-414. https://doi.org/10.1016/j.neuroimage.2010.04.261

Bonnet-Brilhault, F., Rajerison, T. A., Paillet, C., Guimard-Brunault, M., Saby, A., Ponson, L., . . . Roux, S. (2018). Autism is a prenatal disorder: Evidence from late gestation brain overgrowth. *Autism Res*, *11*(12), 1635-1642. https://doi.org/10.1002/aur.2036

Browne, V. A., Julian, C. G., Toledo-Jaldin, L., Cioffi-Ragan, D., Vargas, E., & Moore, L. G. (2015). Uterine artery blood flow, fetal hypoxia and fetal growth. *Philos Trans R Soc Lond B Biol Sci*, *370*(1663), 20140068. https://doi.org/10.1098/rstb.2014.0068

Carré, A., Klausner, G., Edjlali, M., Lerousseau, M., Briend-Diop, J., Sun, R., . . . Robert, C. (2020). Standardization of brain MR images across machines and protocols: bridging the gap for MRI-based radiomics. *Sci Rep*, *10*(1), 12340. https://doi.org/10.1038/s41598-020-69298-z

Cetin, I., & Antonazzo, P. (2009). The role of the placenta in intrauterine growth restriction (IUGR). *Z Geburtshilfe Neonatol*, *213*(3), 84-88. https://doi.org/10.1055/s-0029-1224143

Chen, L., Li, Q., Zheng, D., Jiang, H., Wei, Y., Zou, L., . . . Qiao, J. (2020). Clinical Characteristics of Pregnant Women with Covid-19 in Wuhan, China. *N Engl J Med*. https://doi.org/10.1056/NEJMc2009226

Clausi, S., Coricelli, G., Pisotta, I., Pavone, E. F., Lauriola, M., Molinari, M., & Leggio, M. (2015). Cerebellar damage impairs the self-rating of regret feeling in a gambling task. *Front Behav Neurosci*, *9*, 113. https://doi.org/10.3389/fnbeh.2015.00113

Cohen, J. (1960). A coefficient of agreement for nominal scales. *Educational and psychological measurement*, *20*(1), 37-46.

Czarzasta, K., Makowska-Zubrycka, M., Kasarello, K., Skital, V. M., Tyszkowska, K., Matusik, K., . . . Sajdel-Sulkowska, E. M. (2019). A rat model to study maternal depression during pregnancy and postpartum periods, its comorbidity with cardiovascular diseases and neurodevelopmental impact in the offspring. *Physiol Behav*, *199*, 258-264. https://doi.org/10.1016/j.physbeh.2018.11.024

Czarzasta, K., Wojciechowska, M., Segiet-Swiecicka, A., Borodzicz-Jazdzyk, S., Niedziela, M., & Sajdel-Sulkowska, E. M. (2020). The effect of depressive-like behavior in pregnant rat dams on the cardiovascular system in their offspring. *Stress*, 1-7. https://doi.org/10.1080/10253890.2020.1845646

Damhuis, S. E., Ganzevoort, W., & Gordijn, S. J. (2021). Abnormal Fetal Growth: Small for Gestational Age, Fetal Growth Restriction, Large for Gestational Age: Definitions and Epidemiology. *Obstet Gynecol Clin North Am*, *48*(2), 267-279. https://doi.org/10.1016/j.ogc.2021.02.002

Dehghani, N., & Wimmer, R. D. (2019). A Computational Perspective of the Role of the Thalamus in Cognition. *Neural Comput*, *31*(7), 1380-1418. https://doi.org/10.1162/neco_a_01197

Dubois, J., Dehaene-Lambertz, G., Kulikova, S., Poupon, C., Hüppi, P. S., & Hertz-Pannier, L. (2014). The early development of brain white matter: a review of imaging studies in fetuses, newborns and infants. *Neuroscience*, *276*, 48-71. https://doi.org/10.1016/j.neuroscience.2013.12.044

Ebner, M., Wang, G., Li, W., Aertsen, M., Patel, P. A., Aughwane, R., . . . Vercauteren, T. (2020). An automated framework for localization, segmentation and super-resolution reconstruction of fetal brain MRI. *Neuroimage*, *206*, 116324. https://doi.org/10.1016/j.neuroimage.2019.116324

Fleiss, B., Wong, F., Brownfoot, F., Shearer, I. K., Baud, O., Walker, D. W., . . . Tolcos, M. (2019). Knowledge Gaps and Emerging Research Areas in Intrauterine Growth Restriction-Associated Brain Injury. *Front Endocrinol (Lausanne)*, *10*, 188. https://doi.org/10.3389/fendo.2019.00188

Gholipour, A., Rollins, C. K., Velasco-Annis, C., Ouaalam, A., Akhondi-Asl, A., Afacan, O., . . . Warfield, S. K. (2017). A normative spatiotemporal MRI atlas of the fetal brain for automatic segmentation and analysis of early brain growth. *Sci Rep*, *7*(1), 476. https://doi.org/10.1038/s41598-017-00525-w

Hardan, A. Y., Girgis, R. R., Adams, J., Gilbert, A. R., Keshavan, M. S., & Minshew, N. J. (2006). Abnormal brain size effect on the thalamus in autism. *Psychiatry Res*, *147*(2-3), 145-151. https://doi.org/10.1016/j.pscychresns.2005.12.009

Jenkinson, M., Beckmann, C. F., Behrens, T. E., Woolrich, M. W., & Smith, S. M. (2012). FSL. *Neuroimage*, *62*(2), 782-790. https://doi.org/10.1016/j.neuroimage.2011.09.015

Joyeux, L., De Bie, F., Danzer, E., Van Mieghem, T., Flake, A. W., & Deprest, J. (2018). Safety and efficacy of fetal surgery techniques to close a spina bifida defect in the fetal lamb model: A systematic review. *Prenat Diagn*, *38*(4), 231-242. https://doi.org/10.1002/pd.5222

Kleesiek, J., Urban, G., Hubert, A., Schwarz, D., Maier-Hein, K., Bendszus, M., & Biller, A. (2016). Deep MRI brain extraction: A 3D convolutional neural network for skull stripping. *Neuroimage*, *129*, 460-469. https://doi.org/10.1016/j.neuroimage.2016.01.024

Klein, A., Andersson, J., Ardekani, B. A., Ashburner, J., Avants, B., Chiang, M. C., . . . Parsey, R. V. (2009). Evaluation of 14 nonlinear deformation algorithms applied to human brain MRI registration. *Neuroimage*, *46*(3), 786-802. https://doi.org/10.1016/j.neuroimage.2008.12.037

Koziol, L. F., Budding, D., Andreasen, N., D'Arrigo, S., Bulgheroni, S., Imamizu, H., . . . Yamazaki, T. (2014). Consensus paper: the cerebellum's role in movement and cognition. *Cerebellum*, *13*(1), 151-177. https://doi.org/10.1007/s12311-013-0511-x

Kuklisova-Murgasova, M., Quaghebeur, G., Rutherford, M. A., Hajnal, J. V., & Schnabel, J. A. (2012). Reconstruction of fetal brain MRI with intensity matching and complete outlier removal. *Med Image Anal*, *16*(8), 1550-1564. https://doi.org/10.1016/j.media.2012.07.004

Limperopoulos, C., Bassan, H., Gauvreau, K., Robertson, R. L., Sullivan, N. R., Benson, C. B., . . . duPlessis, A. J. (2007). Does cerebellar injury in premature infants contribute to the high prevalence of long-term cognitive, learning, and behavioral disability in survivors? *Pediatrics*, *120*(3), 584-593. https://doi.org/10.1542/peds.2007-1041

Makropoulos, A., Counsell, S. J., & Rueckert, D. (2018). A review on automatic fetal and neonatal brain MRI segmentation. *Neuroimage*, *170*, 231-248. https://doi.org/10.1016/j.neuroimage.2017.06.074

Miller, S. L., Huppi, P. S., & Mallard, C. (2016). The consequences of fetal growth restriction on brain structure and neurodevelopmental outcome. *J Physiol*, *594*(4), 807-823. https://doi.org/10.1113/JP271402

Moffat, J. J., Ka, M., Jung, E. M., & Kim, W. Y. (2015). Genes and brain malformations associated with abnormal neuron positioning. *Mol Brain*, *8*(1), 72. https://doi.org/10.1186/s13041-015-0164-4

Nosarti, C., Reichenberg, A., Murray, R. M., Cnattingius, S., Lambe, M. P., Yin, L., . . . Hultman, C. M. (2012). Preterm birth and psychiatric disorders in young adult life. *Arch Gen Psychiatry*, *69*(6), E1-8. https://doi.org/10.1001/archgenpsychiatry.2011.1374

Pradhan, S., Kapse, K., Jacobs, M., Niforatos-Andescavage, N., Quistorff, J. L., Lopez, C., . . . Limperopoulos, C. (2020). Non-invasive measurement of biochemical profiles in the healthy fetal brain. *Neuroimage*, *219*, 117016. https://doi.org/10.1016/j.neuroimage.2020.117016

Rajchl, M., Baxter, J. S., McLeod, A. J., Yuan, J., Qiu, W., Peters, T. M., & Khan, A. R. (2016). Hierarchical max-flow segmentation framework for multi-atlas segmentation with Kohonen self-organizing map based Gaussian mixture modeling. *Med Image Anal*, *27*, 45-56. https://doi.org/10.1016/j.media.2015.05.005

Ramphal, B., Pagliaccio, D., Thomas, L. V., He, X., & Margolis, A. E. (2021). Contributions of Cerebellar White Matter Microstructure to Social Difficulty in Nonverbal Learning Disability. *Cerebellum*. https://doi.org/10.1007/s12311-021-01265-4

Rathbone, R., Counsell, S. J., Kapellou, O., Dyet, L., Kennea, N., Hajnal, J., . . . Edwards, A. D. (2011). Perinatal cortical growth and childhood neurocognitive abilities. *Neurology*, *77*(16), 1510-1517. https://doi.org/10.1212/WNL.0b013e318233b215

Rutherford, M., Jiang, S., Allsop, J., Perkins, L., Srinivasan, L., Hayat, T., . . . Hajnal, J. (2008). MR imaging methods for assessing fetal brain development. *Dev Neurobiol*, *68*(6), 700-711. https://doi.org/10.1002/dneu.20614

Sacchi, C., Marino, C., Nosarti, C., Vieno, A., Visentin, S., & Simonelli, A. (2020). Association of Intrauterine Growth Restriction and Small for Gestational Age Status With Childhood Cognitive Outcomes: A Systematic Review and Meta-analysis. *JAMA Pediatr*, *174*(8), 772-781. https://doi.org/10.1001/jamapediatrics.2020.1097

Salehi, M., Karbasi, A., Shen, X., Scheinost, D., & Constable, R. T. (2018). An exemplar-based approach to individualized parcellation reveals the need for sex specific functional networks. *Neuroimage*, *170*, 54-67. https://doi.org/10.1016/j.neuroimage.2017.08.068

Schmahmann, J. D. (2004). Disorders of the cerebellum: ataxia, dysmetria of thought, and the cerebellar cognitive affective syndrome. *J Neuropsychiatry Clin Neurosci*, *16*(3), 367-378. https://doi.org/10.1176/jnp.16.3.367

Sharma, D., Shastri, S., & Sharma, P. (2016). Intrauterine Growth Restriction: Antenatal and Postnatal Aspects. *Clin Med Insights Pediatr*, *10*, 67-83. https://doi.org/10.4137/CMPed.S40070

Smith, F. W., Adam, A. H., & Phillips, W. D. (1983). NMR imaging in pregnancy. *Lancet*, *1*(8314-5), 61-62. https://doi.org/10.1016/s0140-6736(83)91588-x

Straughen, J. K., Misra, D. P., Divine, G., Shah, R., Perez, G., VanHorn, S., . . . Salafia, C. M. (2017). The association between placental histopathology and autism spectrum disorder. *Placenta*, *57*, 183-188. https://doi.org/10.1016/j.placenta.2017.07.006

Subramanian, L., Calcagnotto, M. E., & Paredes, M. F. (2019). Cortical Malformations: Lessons in Human Brain Development. *Front Cell Neurosci*, *13*, 576. https://doi.org/10.3389/fncel.2019.00576

Thomason, M. E. (2020). Development of Brain Networks In Utero: Relevance for Common Neural Disorders. *Biol Psychiatry*, *88*(1), 40-50. https://doi.org/10.1016/j.biopsych.2020.02.007

Thomason, M. E., Grove, L. E., Lozon, T. A., Vila, A. M., Ye, Y., Nye, M. J., . . . Romero, R. (2015). Age-related increases in long-range connectivity in fetal functional neural connectivity networks in utero. *Dev Cogn Neurosci*, *11*, 96-104. https://doi.org/10.1016/j.dcn.2014.09.001

Thomason, M. E., Hect, J., Waller, R., Manning, J. H., Stacks, A. M., Beeghly, M., . . . Romero, R. (2018). Prenatal neural origins of infant motor development: Associations between fetal brain and infant motor development. *Dev Psychopathol*, *30*(3), 763-772. https://doi.org/10.1017/S095457941800072X

Turk, E., van den Heuvel, M. I., Benders, M. J., de Heus, R., Franx, A., Manning, J. H., . . . van den Heuvel, M. P. (2019). Functional Connectome of the Fetal Brain. *J Neurosci*, *39*(49), 9716-9724. https://doi.org/10.1523/JNEUROSCI.2891-18.2019

Wells, E. M., Walsh, K. S., Khademian, Z. P., Keating, R. F., & Packer, R. J. (2008). The cerebellar mutism syndrome and its relation to cerebellar cognitive function and the cerebellar cognitive affective disorder. *Dev Disabil Res Rev*, *14*(3), 221-228. https://doi.org/10.1002/ddrr.25

Werner, H., Gasparetto, T. D., Daltro, P., Leandro Gasparetto, E., & Araujo Júnior, E. (2018). Typical lesions in the fetal nervous system: correlations between fetal magnetic resonance imaging and obstetric ultrasonography findings. *Ultrasonography*, *37*(3), 261-274. https://doi.org/10.14366/usg.17040

Wheelock, M. D., Hect, J. L., Hernandez-Andrade, E., Hassan, S. S., Romero, R., Eggebrecht, A. T., & Thomason, M. E. (2019). Sex differences in functional connectivity during fetal brain development. *Dev Cogn Neurosci*, *36*, 100632. https://doi.org/10.1016/j.dcn.2019.100632

Wu, Y., Lu, Y. C., Jacobs, M., Pradhan, S., Kapse, K., Zhao, L., . . . Limperopoulos, C. (2020). Association of Prenatal Maternal Psychological Distress With Fetal Brain Growth, Metabolism, and Cortical Maturation. *JAMA Netw Open*, *3*(1), e1919940. https://doi.org/10.1001/jamanetworkopen.2019.19940

Yamashita, R., Nishio, M., Do, R. K. G., & Togashi, K. (2018). Convolutional neural networks: an overview and application in radiology. *Insights Imaging*, *9*(4), 611-629. https://doi.org/10.1007/s13244-018-0639-9

Zauche, L. H., Darcy Mahoney, A. E., & Higgins, M. K. (2017). Predictors of Co-occurring Neurodevelopmental Disabilities in Children With Autism Spectrum Disorders. *J Pediatr Nurs*, *35*, 113-119. https://doi.org/10.1016/j.pedn.2017.04.002

Zhang, P., Ha, T., Larouche, M., Swanson, D., & Goldowitz, D. (2015). Kruppel-Like Factor 4 Regulates Granule Cell Pax6 Expression and Cell Proliferation in Early Cerebellar Development. *PLoS One*, *10*(7), e0134390. https://doi.org/10.1371/journal.pone.0134390

Ethics approval

Date: 27 May 2020

To: Dr Emma Duerden

Project ID: 115440

Study Title: FIND: Fetal Imaging and NeuroDevelopment study

Application Type: HSREB Initial Application

Review Type: Delegated

Meeting Date: 25FEB2020

Date Approval Issued: 27/May/2020 17:16

REB Approval Expiry Date: 27/May/2021

_____

Dear Dr Emma Duerden

The Western University Health Science Research Ethics Board (HSREB) has reviewed and approved the above mentioned study as described in the WREM application form, as of the HSREB Initial Approval Date noted above. This research study is to be conducted by the investigator noted above. All other required institutional approvals must also be obtained prior to the conduct of the study.

Documents Approved:

Document Name	Document Type	Document Date	Document Version
FIND study flyer-2020-03-05	Recruitment Materials	05/Mar/2020	2
Pregnancy Study Robarts Brochure_ 05-03-2020	Recruitment Materials	05/Mar/2020	2
MRI_screening_form	Other Data Collection Instruments	05/Mar/2020	1
Email Return Script 11-03-2020 - V 2.0	Email Script	11/Mar/2020	2
Phone Script - March 20, 2020	Telephone Script	20/Mar/2020	1
REB_protocol_March 20, 2020_V3	Protocol	20/Mar/2020	3
DCF_V3_03-20-2020	Other Data Collection Instruments	20/Mar/2020	3
FIND Master List_2020_03-20_V1	Other Data Collection Instruments	20/Mar/2020	1
Internet Advertisement	Recruitment Materials	02/Apr/2020	1
LOI_Maternal_2020-05-27_v6	Written Consent/Assent	27/May/2020	6

Documents Acknowledged:

Document Name	Document Type	Document Date	Document Version
FIND_budget	Study budget	07/Feb/2020	1

No deviations from, or changes to, the protocol or WREM application should be initiated without prior written approval of an appropriate amendment from Western HSREB , except when necessary to eliminate immediate hazard(s) to study participants or when the change(s) involves only administrative or logistical aspects of the trial.

REB members involved in the research project do not participate in the review, discussion or decision.

The Western University HSREB operates in compliance with, and is constituted in accordance with, the requirements of the TriCouncil Policy Statement: Ethical Conduct for Research Involving Humans (TCPS 2); the International Conference on Harmonisation Good Clinical Practice Consolidated Guideline (ICH GCP); Part C,

Division 5 of the Food and Drug Regulations; Part 4 of the Natural Health Products Regulations; Part 3 of the Medical Devices Regulations and the provisions of the Ontario Personal Health Information Protection Act (PHIPA 2004) and its applicable regulations. The HSREB is registered with the U.S. Department of Health & Human Services under the IRB registration number IRB 00000940.

Please do not hesitate to contact us if you have any questions.

Sincerely,

Nicola Geoghegan-Morphet, Ethics Officer on behalf of Dr. Joseph Gilbert, HSREB Chair

Note: This correspondence includes an electronic signature (validation and approval via an online system that is compliant with all regulations).

Curriculum vitae

JIANAN WANG

<u>EDUCATION</u>

Master of Engineering Science, Biomedical Engineering

- The University of Western Ontario | Feb 2022 (approx.)

Bachelor of Science, Honors Specialization in Computer Science

- The University of Western Ontario | May 2019

<u>WORK EXPERIENCE</u>

- **<u>Editor & photographer, SEPTDAYS media company, Montreal, QC | May 2018 – August 2018</u>**

o Retrieved English articles from news websites and translated them for release

o Edited the report and photos for the 'Exhibition of Immigration and Integration in Quebec' event

o Edited recorded videos and photos for a seminar between Septdays and Radio Canada International

<u>PEER-REVIEWED PUBLICATIONS</u>

1. Seguin D, Pac S, **Wang J,** Nicolson R, Martinez-Trujillo J, Duerden, EG**.** Longitudinal development of the amygdala subnuclei in adolescents with autism spectrum disorder and the association with symptomatology. Brain & Behaviour 2021 *Published.* [PMID](#)*: 34333868*

2. Pac S, Seguin D, **Wang J**, Nicolson R, Martinez-Trujillo J, Anagnostou E, Schachar R, Crosbie J, Lerch JP, Hammill C, Kelley E, Ayub M, Liu X, Brian J, Georgiades, S. Duerden, EG. Amygdala subnuclei volumes predict anxiety in children with autism spectrum disorders, attention deficit hyperactivity disorder and obsessive-compulsive disorder. *Scientific Reports*. *Revisions requested.*

<u>CONFERENCE PUBLICATIONS</u>

1. **Jianan Wang,** Emily S. Nichols, Megan Mueller, Barbra de Vrijer, Roy Eagleson, Charles A. McKenzie, Sandrine de Ribaupierre, Emma G. Duerden. Automatic subcortical structures segmentation in fetal MRI using template-based registration. London Health Research Day 2021.

2. Diane Seguin, Sara Pac, **Jianan Wang**, Rob Nicolson, Julio Martinez-Trujillo, Emma G. Duerden. Social and repetitive behaviours in youth with Autism Spectrum Disorder and the association with amygdala subnuclei maturation. *International Association for the Study of Autism*. Published. 2021

3. Diane Seguin, Sara Pac, **Jianan Wang**, Rob Nicolson, Julio Martinez-Trujillo, Emma G. Duerden Maturation of the amygdala subnuclei in children and adolescents with Autism Spectrum Disorder and the association with social and repetitive behaviours. *Society for Neuroscience, Global Connectome*. Published. 2020

4. Noah Brierley, Sara Pac, **Jianan Wang**, Diane Seguin, Robert Nicolson, Julio Martinez-Trujillo, Evdokia Anagnostou, Jason Lerch, Chris Hammill, Elizabeth Kelley, Muhammed Ayub, Jessica Brian, Emma Duerden. Early life adversity and hippocampal maturation in children with autism spectrum disorders. Human Brain Mapping 2020, Montreal, QC. *Published.*

5. Diane Seguin, **Jianan Wang**, Rob Nicolson, Julio Martinez-Trujillo, Emma G. Duerden. Lateral and central nuclei volumes predict anxiety and depression scores in children with neurodevelopmental disorders. (2019) Society for Neuroscience, Chicago, IL. *Published.*

6. Diane Seguin, **Jianan Wang**, Rob Nicolson, Julio Martinez-Trujillo, Emma G. Duerden. Free and Constrained gaze differentially activate the amygdala in individuals with and without Autism Spectrum Disorders. (2019) International Association for the Study of Autism. *Published.*

7. Diane Seguin, **Jianan Chen**, Rob Nicolson, Julio Martinez-Trujillo, Emma G. Duerden. Free and Constrained gaze differentially activate the amygdala in individuals with and without Autism Spectrum Disorders. (2019) Neuroscience Research Day, London, Ontario. *Published.*

PROJECTS EXPERIENCE

- **Graduate Thesis Project**

Automatic segmentation of fetal brain structures from high-field magnetic resonance imaging.

o Applied an existing automatic fetal brain segmentation algorithm (*NiftyMIC* software) on brain structures from MRI images

o Applied linear and nonlinear image registration techniques for fetal deep brain structures segmentations

o Tested the reliability of the fetal deep brain structure segmentation pipeline against the manual segmentation method

- **Undergraduate Thesis Project**

Automatic segmentation of brain structures from high-field magnetic resonance imaging.

o Applied an existing automatic segmentation algorithm (*Freesurfer* software) on brain structures from MRI images

o Tested the reliability of this algorism against the manual segmentation method on a child population ages 7-12 with mental development disorders

- **Jamming (personal side project)**

A web-based application that implements Spotify API. It allows the users to log in to search for songs/artists/albums, and to save the searched songs into a new playlist under the account.

o GitHub repository: *https://bit.ly/2N3RDoF*

- o Self-taught and used JavaScript and React
- o Another similar personal project (Ravenous) can be found at GitHub repository: *https://bit.ly/2Qqh4yK*

- **Phillips Hue Lights (group project)**

A web-based application that interfaces with Phillips Hue Lighting system to give users control over their Phillips bulbs (used language C++ and framework Web toolkit).

- o (The bitbucket team repository is kept private)
- o Designed the project plan
- o Handled the HTTP requests based on Phillips Hue API
- o Interacted between server-side and client-side works
- o Encouraged teammates to communicate their workflows and helped teammates to understand the Web-toolkit documents

- **Explain That Again (group project)**

A web-based educational tool that allows students to ask questions on the lecture and get answers in chat room in real-time (used Groovy).

- o GitHub project site: *https://bit.ly/2NikKQp*
- o Designed the project using UML and set small goals for project planning
- o Integrated back-end and front-end work and UI design

TECHNICAL SKILLS

- The University of Western Ontario | Feb 2022 (approx.)
- Programming languages: Python, Java, C, C++, Ruby, HTML, CSS, JavaScript, PHP
- Database: PostgreSQL
- Familiar with Git
- Morphological image processing (image normalization and segmentation)
- Quick learning and transitioning of programming languages